Design and Manufacturing Analysis of Resonantly Coupled Circuits and Other Components used for Applied Wireless Power Transmission: Application Analysis

by

Mitchell S. Krogman

B.S. Industrial Engineering
Kettering University, 2012

Submitted to the Department of Mechanical Engineering in partial fulfillment of the requirements for the degree of

MASTER OF ENGINEERING IN MANUFACTURING
AT THE
MASSACHUSETTS INSTITUTE OF TECHNOLOGY

September 2013

Signature of Author: .....

Mitchell S. Krogman
Department of Mechanical Engineering
August 15, 2013

Certified By: .....

Prof. David E. Hardt
Ralph E. and Eloise F. Cross Professor of Mechanical Engineering
Thesis Supervisor

Accepted By: .....

Chairman, Committee for Graduate Students
Department of Mechanical Engineering

Design and Manufacturing Analysis of Resonantly Coupled Circuits and Other Components used for Applied Wireless Power Transmission: Application Analysis

by

Mitchell S. Krogman

Submitted to the Department of Mechanical Engineering on August 15, 2013,
In partial fulfillment of the requirements for the
Degree of Masters of Engineering in Manufacturing

Abstract

This thesis describes the analysis of a locking mechanism designed by ProTeqt Technologies. More specifically, the analysis considers the mechanism after the implementation of a resonantly coupled circuit used to receive and transmit wireless energy. Ultimately, the wireless energy is used to generate heat, which in turn causes a polymeric material to expand, thereby creating a mechanical force to disengage the locking mechanism. The analysis considers the force generated through wireless transmission, as well as the forces required to disengage the locking mechanism. The general physics of wireless energy transmission through resonant coupling is presented, as well as design specifications and manufacturing techniques used to produce the secondary circuit. Force requirements and design specifications that drive the success of the locking mechanism are then discussed before the presentation of coinciding results.

Thesis Supervisor: David E. Hardt
Title: Professor of Mechanical Engineering

For my grandfather,

David O'Brien

Acknowledgements

There are many people that deserve thanks for their contributions to this thesis, both at MIT and ProTeqt Technologies.

I would like to thank professor David Hardt, our thesis advisor, for his understanding, recommendations, and ubiquitous patience. We all opine that he has a knack for making the difficult concepts seem so simple.

Dan Beane, ProTeqt's lead mechanical engineer, and most importantly, electricity and magnetism expert, went above and beyond to facilitate our research. He provided us with insight, resources, time, and attention. Without him, this project truly would not have been possible. It's his persistence for understanding that helped push our research.

George Raniuk, a key stakeholder in ProTeqt helped us gain a practical perspective of the project at hand. He was a straight shooter, who was not hesitant to provide an unbiased opinion, or key advice. His tolerance to questions regarding this project and others, provided great insight into the world of start-ups.

My teammates were absolutely essential to the success of this project. We truly were a diverse group, together, spanning three continents. Their mechanical and, cumulative, electrical intuition helped raise many questions leading to key discoveries. I have learned so much from an engineering and cultural standpoint over the course of this project: Thank you Amaury and Tianyu.

Finally, I would like to thank my family. Their unconditional support throughout my experience at MIT and ProTeqt was extremely motivational. Without them, I would likely be on page 1. They helped me push through the tough times, and were always willing to offer advice.

Table of Contents

List of Figures

List of Tables

Chapter 1

Introduction

1.1 General Research Topic

The foundation of this thesis is centered around ProTeqt Technologies, a company dedicated to providing anti-theft devices (know as "benefit denial solutions") for the electronics retail industry. In particular, we are developing a technique that can be used to expand their product functionality, based upon a mechanical locking mechanism for a Micro USB port. More explicitly, we are developing components and understanding parameters that will increase the distance from a disabling device that their technology can be used by extending a magnetic field via resonant coupling and understanding the interactions within their product.

1.2 Need for Benefit Denial Solutions against Retail Theft

Global retail theft has increased dramatically in recent years, driven by the expansion of online marketplaces [1]. Large online market places such as Ebay have given rise to organized retail theft. These online markets make buying and selling stolen items easier than ever. Despite huge investments from retailers and manufacturers (more than $28 billion in 2011 [2]), this plague has continued to grow steadily. The most common solution to prevent theft in retail stores is an electronic article surveillance (EAS) system that will alert a retailer if a product passes through the doors prior to purchase. EAS systems have the limitation that the retailer still has to respond to the alert and this response is often hesitant. In some cases, retailers explicitly tell their employees not to confront those suspected of theft. Increased shrinkage, coupled with non-effective EAS systems, has lead retailers to restrict consumer access for high-theft products (e.g. locking glass or back room cages). However, these actions are known to significantly decrease sales. Moreover, these solutions attempt to address theft only at the point of sale. They fail to address the largest component of shrinkage in the retail industry: organized theft throughout the supply chain (53% of theft in North America [2]).

As a result, retailers are looking for solutions that will provide more security than the current theft prevention methods. They are interested in eliminating the motivation to steal: the resale or use of the product. ProTeqt Technologies has addressed this solution by developing a new type of mechanical lock system that temporarily disables the product, rendering it unusable until it is legally purchased. At the point-of-sale, a deactivating tablet recognizes the product using a RFID tag embedded in the packaging. It then emits a certain electromagnetic signal, based on the product, that deactivates the mechanical lock. If the product is stolen, the lock cannot be removed without damaging the product. Furthermore, their solution can also be easily integrated with current EAS systems using the existing RFID tag.

1.3 Product Components and Performance

ProTeqt's system is comprised of three key components: the deactivation tablet, cloud database, and mechanical lock. The research covered by this thesis focuses on two of the three elements: the deactivation tablet and the mechanical lock. However, to fully understand ProTeqt's technology and the sequence of events that takes place, we must briefly consider all three components.

At the point of sale, the sales clerk first scans the product containing ProTeqt's lock. The RFID is then recognized, allowing the system to look up data corresponding to that particular product in the ProTeqt database. If the product has not previously been unlocked, a certain frequency is gathered from the cloud database that coincides with the product at hand. The clerk then positions the product in such a way that the lock is directly over the center of the tablet. With the product in position, the tablet creates a strong electromagnetic field at the appropriate frequency to deactivate the mechanical lock. The customer takes the product home, and uses his or her product as if the lock was never there. They are able to simply remove the lock and throw it away.

1.3.1 Deactivation Tablet

The deactivation tablet is a highly integrated computer system. It uses RFID detection to recognize products, an Internet connection to access the cloud database, LED

lights to guide the product to the center of the tablet, a function generator to produce certain frequencies, and finally a large coil to generate an electromagnetic field. The tablet must be small and unobtrusive to provide easy integration at the point of sale.

ProTeqt has contracted the design and manufacturing of the deactivation tablet to MACK Technologies[1], whose expertise is in circuit board and complex system assembly. While we may not be designing or analyzing the system for manufacturability, we need to understand the full functionality and design parameters of the deactivation tablet to further understand the effects it has on other components like the mechanical lock.

1.3.2 Mechanical Lock

The mechanical lock is a small device that is added to a consumer product at the manufacturing site. The lock is designed to eliminate key features of a product. By encapsulating and interacting with the consumer product, both internally and externally, the device is completely protected from use if it's not legally purchased. Inside, the lock contains a mechanism that will disengage itself from the internal portion of the product. When activated, a spring forces the lock off the product inside the packaging. This action is completed at the point of sale.

The lock design is highly dependent on key product features that can be used to render the product unusable. At the time of this project, locks have been designed for two product lines: USB thumb drives and CD-type disks (Figure 1). For the USB thumb drives, the lock is attached to the male plug. An improper attempt to remove the lock will permanently damage the plug, rendering the thumb drive useless. For the disks, the lock secures the disk to its case. Here, improper removal will simply break the disk or the packaging. In both scenarios the disk and packaging are not separated. The lock was designed so that the case or disk would break before the lock, which joins the two.

ProTeqt has developed several prototypes and working models of mechanical locking systems for a plethora of devices: from perfume to video games. A micro USB lock system will be analyzed throughout the extent of this thesis. This lock has been identified as a critical mechanism that will facilitate growth and opportunities for

[1] 27 Carlisle Road, Westford, MA 01886

ProTeqt, because the micro USB port is used on many different types of devices to both power, and transfer data.

Figure 1: The thumb drive lock (Left) and the CD-disk lock (right). Locking mechanisms are identified by the pad-lock symbol.

The current design for the micro USB lock uses a number of moving parts, including plastics, springs, and sheet metal encapsulated by an external plastic housing. Previously, ProTeqt's most successful lock has been a standard USB lock. This lock is substantially simpler, using only plastic to create the lock. The standard USB interface is much larger than the micro USB components, which also encourages a simpler design.

A simplified diagram explaining the interaction of the components inside the micro USB lock is shown in Figure 2. We are limited in our discussion for purposes of confidentiality. The basic components inside the lock are the LC circuit (discussed in chapter 5), enabler, spring, and sheet metal components. For a product to be successfully unlocked, the enabler must produce a force inside the lock that bends a small sheet metal component. The sheet metal component (sheet metal 1) must be displaced until the small lip clears the second sheet metal component. At this point, a spring forces the first sheet metal component through the second, disengaging the lock. This displacement is identified in Figure 2.

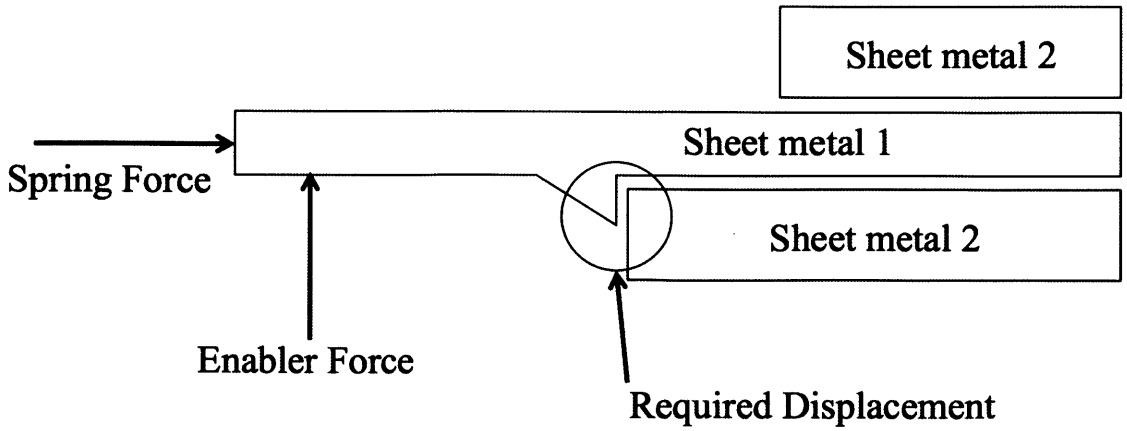

Figure 2: Internal diagram of the micro USB lock system.

The enabler is the most important component in the lock. It expands when inductively heated (Chapter 2). The whole system depends on the enabler expanding enough to fire the unlatching device when it receives energy from the deactivation tablet. The basic dimensions of the full sized enabler are 12mm by 9mm, and about 0.3mm thick. Upon heating, the enabler can expand to nearly forty times its original size. The enabler consists of a polymeric material that is sandwiched between two sheets of metal foil. When on the tablet, the enabler intersects with lines of flux produced by the primary coil. These lines of flux generate eddy currents that inherently produce heat. When the parameters are correct, it's this heat that forces the enabler to expand, exerting a force on the other components in the lock.

1.3.3 Improving Product Performance

ProTeqt has complete control over their mechanical locking device and deactivation tablet, but they must be compatible with many types of locking methods (eg. USB, disk, etc.) and packaging. In the case of the USB thumb drives (Figure 4) and the disks, the packaging is very slim, allowing the lock to be close to the deactivation tablet. Once the magnetic field is created, the lock is easily deactivated. Products that are embedded in thicker packaging (Figure 3) have proven to be more difficult to unlock because the magnetic field degrades rapidly with distance. ProTeqt has begun to

investigate solutions that will permit deactivation of the mechanical lock at a distance of 1 inch from the tablet.

ProTeqt, having developed two unique applications for their technology (USB tumb drive, and CD-type disk), is ready to move forward with the development for a, new, Micro USB lock. This lock will perform similarly to the USB thumb drive lock, in that it will interface with the consumer product internally. The Micro USB port uses a smaller profile than the standard USB port, introducing some new design challenges. However, the Micro USB lock is used far more prevalently and with more expensive products than the standard USB. Moving forward, ProTeqt would like to achieve the functionality of the Micro USB lock at 1 inch above the tablet surface.

Figure 3: External hard drive with thick packaging requires a stronger field. This packaging, being targeted by ProTeqt, leaves the lock at 1 inch above the tablet.

Figure 4: USB thumb drive packaging. Because the packaging is thin, the lock is very close to the primary coil and deactivation is easy.

1.4 Induction Heating

The most important concept of ProTeqt's current design is induction heating. They use this phenomenon to generate heat inside the lock; thereby causing a polymeric material to expand, which in turn creates a force that disengages the lock from the product. The principals of induction heating are applied from the tablet to the enabler. To simplify things, the tablet can be thought of as an induction cook top, and the enabler a pot. The main purpose of the deactivation tablet is to heat the enabler. More information on induction heating is discussed in Chapter 2.

1.5 Resonant Coupling

As stated above, the objective of ProTeqt is to achieve unlocking at one inch from the tablet. Among several potential solutions, ProTeqt chose to explore and implement the effects of resonant inductive coupling. Resonant inductive coupling is a means to transfer wireless energy through two coils that are tuned to resonate at the same frequency. We can effectively use resonant inductive coupling to extend the magnetic field created by the deactivation tablet. In reality we can create a new magnetic field

using the energy transferred wirelessly from the original field created by the tablet. Using a field that is closer to the mechanical lock will increase the effectiveness, and decrease the decaying effects of the field at distance. Furthermore, this solution will allow ProTeqt to postpone a redesign of the deactivation tablet. Instead, a simple component can be designed that will allow the wireless transfer of energy: an LC circuit.

1.6 Design and Production of LC Circuits

To extend the field, we need to develop an LC circuit. An LC circuit is a circuit comprises an inductor and a capacitor. This circuit is typically drawn as shown in Figure 5. By placing the small circuit inside the mechanical lock, we can create a new magnetic field inside the lock. Although an LC circuit is simple (an inductor coil connected to a capacitor), it should be designed to work at maximum efficiency. The circuit can be tuned to operate most efficiently at a certain frequency. However, because the LC circuit will be operating inside the mechanical lock, we must consider the interaction and effects of the existing components of the lock. Moreover, the performance of the circuit is dependent on the quality of manufacturing. Thus, the effects of manufacturing variability must be understood, controlled, and minimized.

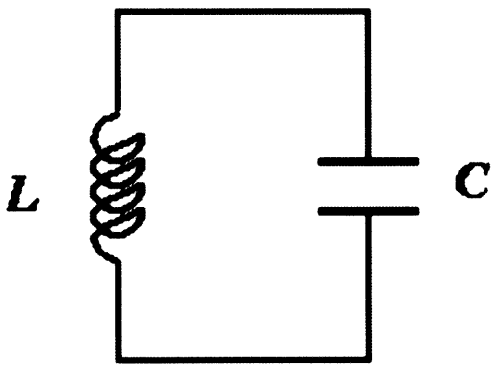

Figure 5: Typical diagram for an LC circuit where L is the inductor and C is the capacitor.

Finally, because the circuit is inside the lock, it is disposable and must be manufactured at low cost. The volume of the circuits is on the order of millions of units

per year. The production rate and cost are two important parameters that must be considered and accounted for in the beginning stages of the design.

1.7 Problem Statement

The problem statement developed by ProTeqt for our thesis project was to understand the interactions between the deactivation tablet, LC circuit, and mechanical lock to optimize and, moreover, recommend a final design of the LC circuit that will excite the enabler at 1 inch above the tablet, thereby disengaging the lock, at a manufacturing cost of $0.05.

Building on this problem statement, the goal of the project is to develop an LC circuit that will effectively extend the application of ProTeqt's benefit denial solution from zero to one inch using resonant inductive coupling. Furthermore, the forces and interactions between the LC circuit, enabler, and mechanical lock were understood to provide a better understanding of ProTeqt's entire benefit denial solution. Multiple challenges were addressed, from theoretical physics to manufacturing issues. This thesis considers the topics we faced while working at ProTeqt. It must be noted that some tasks were distributed among ProTeqt's partners and are out of the scope of this thesis.

This project was conducted through three phases. In the first phase we worked to understand, characterize, and recommend and optimal design for an LC circuit to permit the transfer of wireless energy. For this phase it was necessary to understand the principle of induction heating, the physical mechanisms required to create a new magnetic field, and the parameters for optimizing the design of an LC circuit.

In the second phase, the unlocking mechanism was analyzed to understand the interaction between the mechanical parts and the circuit. The purpose of this stage is to obtain and understand data related to the forces required to disengage the locking mechanism.

Finally, in the last phase of the project, the effect of manufacturing variability and the variability of the components in the lock were analyzed to understand the likelihood of failure and the likely source of these failures.

1.8 Task Division

Based upon the three phases of the approach, tasks were divided among the three group members: Amaury Rony, Tianyu Zhu, and myself. Even though the thesis project at hand has been completed by the collective group, each team member took the lead on one of the three phases, and delegated the responsibility for tasks essential for completion as needed. Theoretical physics and coil design was under the responsibility of Amaury. I led the work on the unlocking mechanism and its interaction with the LC circuit including the forces acting on and required by the lock. Finally, Tianyu took responsibility of the manufacturing variation.

Chapter 2

Induction Heating

2.1 Principals of Induction Heating

Induction heating is a method to heat an electrically conducting object using electromagnetic induction. An induction heater consists of an inductor excited with an alternating current. According to Faraday's Law, the changing current creates a changing electromagnetic field around the inductor. When the electrically conducting object is placed inside this field, eddy currents are generated within the conductor. This phenomenon causes Joule heating owing to losses in the conductor. Compared to traditional heating methods, induction heating does not require direct physical contact because the energy is transferred from the heater to the conducting component through electromagnetic waves.

2.1.1 Eddy Current

French scientist Francois Arago first discovered Eddy currents in 1824 [3]. When a conductor is placed in a changing magnetic field, circulating eddies of current are created inside the conductor. The name eddy current is derived from the analogy of circulating water in fluid dynamics. In a non-zero resistivity conductor, the eddy current induced will generate heat, by the concept of Joule heating, and electromagnetic forces. The current induced is greater with either a stronger magnetic field or a higher frequency magnetic field. According Lenz's law, the eddy current will flow in a direction such that the magnetic field created by the current will oppose the magnetic field that induces the current. In other words, the eddy current will create a lesser magnetic field that will cancel part of the primary field.

2.1.2 Skin Effect

In direct current, current density is uniform throughout the entire cross section of the conductor. Alternating current is different. The magnetic field at the center increases as the frequency increases due to the combined effects of conductivity and permeability. The magnetic field creates current in the opposite direction of the current flowing through the conductor, making it more difficult for the current to flow through the center. This resistance is called reactance. Because of the reactance at the center, the current density is the lowest there and largest near the surface of the conductor where the reactance goes to zero. This concentration of current at the surface is named the "Skin Effect".

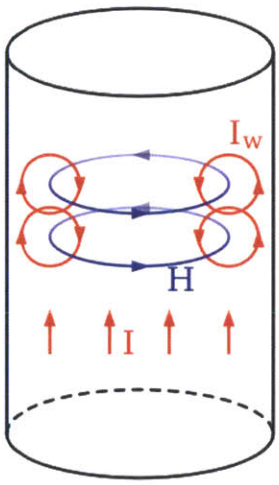

Figure 6: Schematic of current and magnetic field in a conductor with alternating current. I (red arrows) is the current passing through the conductor. It induces the magnetic field H (blue loops), which itself creates the loops of current, I_w.

The AC current density decreases exponentially with the depth from the surface. The skin depth is defined as the distance into a conductor at which is current density falls to 37% of its value along the surface. The skin depth can be expressed as:

$$\delta = \frac{1}{\sqrt{\pi f \mu \sigma}} \tag{2.1}$$

where:

f = frequency, μ = absolute magnetic permeability of the conductor = $\mu_o * \mu_r$,

μ_o = Permeability of air = $4\pi * 10^{-7}$ $\left(\frac{h}{m}\right)$, μ_r = Permeability of the conductor

σ = Conductivity of the material

For example, a copper wire with AC of 220 kHz, will have a skin depth of 0.141mm. This means that 63% of the current flowing in a copper wire will flow within a distance of 0.141mm to the surface. The effective resistance can be calculated as current flowing uniformly through a layer of thickness δ with the DC resistivity of that material. The cross-sectional area can be approximated by [4]:

$$A_{eff} = 2\pi r \cdot \delta \tag{2.2}$$

where: r = radius of the wire

Then, the AC resistance is:

$$R_{AC} \approx R_{DC} \frac{r}{2\delta} \tag{2.3}$$

All the equations shown above are based the assumption that the skin depth is significantly smaller than the radius. By negating this assumption and using a wire diameter on the same order as the skin depth, a resistance at low frequency can be calculated using the following model:

$$R_{low\ freq} \approx R_{dc} + \frac{l}{48\sigma\pi\delta^2} \tag{2.4}$$

where:

l = total length of the wire

To maximize the heating effectiveness, we want to find a proper combination of material properties and material thickness. Optimal heating can be achieved by minimizing the material thickness to a value close to the skin depth.

2.1.3 Selection of Materials and Thickness

The selection of material is critical, because material properties determine the effectiveness of the energy transmission and subsequent heating. Only conductive

materials can be used for induction heating because eddy currents need to flow through the object in order generate heat. Even though eddy currents can occur in any conductor, iron and its alloys respond better than aluminum and copper to induction heating owing to their ferromagnetic nature. Using the same alternating current, ferromagnetic materials have a significantly smaller skin depth, resulting in greater resistance and therefore Joule heating.

For materials that are thinner than their skin depth at the desired frequency, the skin effect is no longer important. The resistance of the material is only determined by the thickness and basic material resistivity. In this case, aluminum and copper can perform just as well as ferromagnetic materials.

Chapter 3

Resonant Inductive Coupling

3.1 Magnetic Field Generated by Current

This section provides an initial background on electromagnetic theory. Based on this introduction, inductive coupling is introduced. ProTeqt uses a large electromagnet in the deactivation tablet to unlock their locks. To extend their deactivation distance from the surface of the tablet to an inch above, resonant inductive coupling has been introduced to the system to permit efficient wireless energy transfer. For more extensive information, the reader can refer to a more detailed handbook like [4].

3.1.1 Magnetic Field Strength at a Coil Axis

Every current, i.e. a flow of moving charges, is associated with a magnetic field with magnitude that is represented by the magnetic field strength, $\vec{B}$ (in Teslas). The magnetic field generated by a line of current within a wire is derived from Biot-Savart law [4]. That is

$$\overrightarrow{B_Q} = \frac{\mu}{4\pi}\int_0^L \frac{\vec{I}dl \times \overrightarrow{1_{QP}}}{QP^2} \qquad (3.1)$$

Where:

Q is the point of observation.

P is the center of the elementary element dl.

$\vec{I}$ indicated the intensity and the direction of the current at P.

$\overrightarrow{1_{QP}}$ is an elementary vector from Q to P.

$\mu = \mu_r\mu_0$ is the permeability of the medium

From this equation, it is possible to find the magnetic field along a single circular loop of radius a, carrying a current I. We are especially interested in the magnetic field $\overrightarrow{B_z}$ along the axis of the loop. It is oriented in the axis direction, as shown on Figure 7:

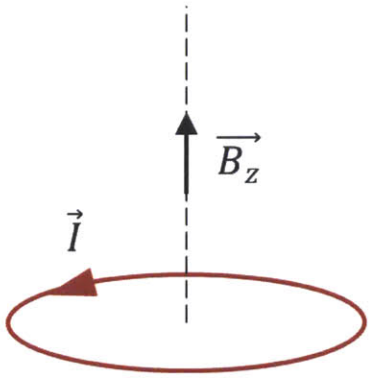

Figure 7: A current-carrying loop and it's associated magnetic field along the central axis.

The magnitude of the field is

$$B_z = |\overrightarrow{B_z}| = \frac{\mu I a^2}{2(z^2 + a^2)^{\frac{3}{2}}} \qquad (3.2)$$

To understand the effect of distance, the magnetic density is plotted as a function of the distance from the hoop (Figure 8), which is a plot of equation 3.2 with a=1 mm and I=1.

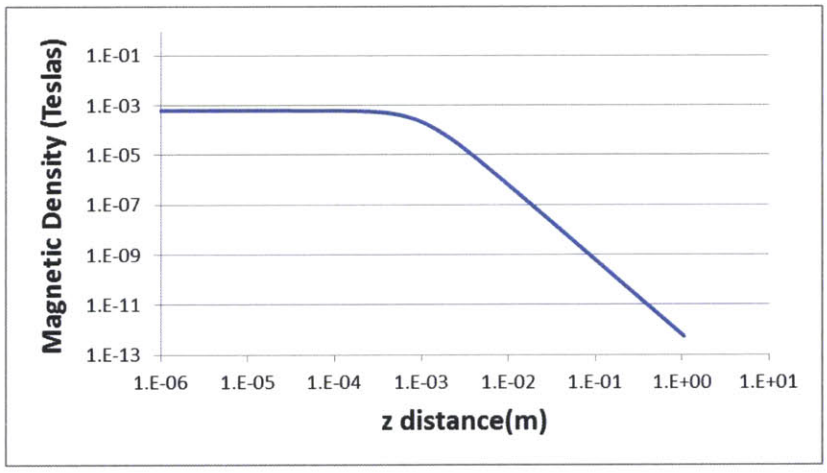

Figure 8: Magnetic Field along the hoop axis, vs. the hoop radius (log-log scale). Hoop radius a= 1 mm and current I is 1 A in eqn 3.2.

As long as the distance from the conductor is less than the radius, the magnetic field remains approximately constant. However the magnetic density decreases rapidly as the measuring point is moved further away from the center of the loop.

As will be discussed below, a flat spiral coil can be used to increase the magnetic field by increasing the number of hoops. A spiral coil can be seen as a certain number of concentric hoops with different radii ($a_1, a_2, a_3 \ldots$), and potentially with N layers. In this case, the total intensity of the magnetic field along the axis of the coil is the superposition of the magnetic field intensities generated by each single loop [5].

3.1.2 Magnetic Flux and Inductance

The line along which the magnetic strength is constant is called a line of magnetic flux. We are interested in the total magnetic flux, i.e. the total number of flux lines passing through a given surface. The magnetic flux Φ is proportional to the field density B and the area:

$$\Phi = B.A \tag{3.3}$$

Going back to the current-carrying hoop, it is now possible to define and calculate its inductance L.

$$L = \frac{\Phi}{I} \tag{3.4}$$

where Φ is the magnetic flux through the inside surface of the loop.

$$L = \frac{\mu\pi\alpha}{2} \tag{3.5}$$

It is noticed that inductance does not depend on the current. Equation 3.5 comes from the RFID handbook [5]. It only depends on the material properties and the geometry layout. The inductance of a spiral coil is the sum of the inductances of each single hoop.

3.2 Inductive Coupling

If a second conductor hoop is located closed to the first one, a portion of the magnetic flux Φ_{21} from the first hoop passes through the second. The two conductors are now inductively coupled. As for inductance (also known as self-inductance), we define the mutual inductance M_{21} of conductor hoop 2 in relation with conductor hoop 1 as:

$$M_{21} = \frac{\Phi_{21}}{I_1} \tag{3.6}$$

In a similar way the mutual inductance of conductor hoop 1 in relation with conductor hoop 2 is:

$$M_{12} = \frac{\Phi_{12}}{I_2} \tag{3.7}$$

It has been shown that both mutual inductances are equal [5] i.e.

$$M_{12} = M_{21} = M \tag{3.8}$$

Continuing with these two coils, we consider the case where the first inductor carries a high frequency, producing a varying magnetic field at the same frequency. With the secondary coil located in the surrounding area so that the two are coupled, Faraday's law states that any change to the magnetic flux generates an electric field, which induces a voltage in the secondary coil. It's this induced voltage that can be used to supply power to another application (RFID chip, transformer, etc.).

3.3 Resonant Coupling

Experience and analysis [6] show that coupling decreases very quickly as the distance between two coils increases. To combat this issue, we add a capacitor to the circuit. This creates a resonance phenomenon that increases the coupling efficiency at a certain frequency. At this frequency, called the resonant or natural frequency, the power

transmission is much more efficient. Thus, the distance between the coils can be substantially increased.

3.4 Applications

The physical phenomena discussed in this chapter can be advantageously used for contactless electronic application. Two of the most important and applicable applications are RFID tags and wireless power. Both applications are used by ProTeqt. Before the deactivation of the lock, the product is recognized by its RFID tag, inside the package. Then, the principles of wireless power transmission will be used in order to increase the maximum distance of deactivation.

3.4.1 RFID

Today many companies, large and small, use automatic identification systems, or Auto-ID, for a large range of applications; including inventory management, sales and purchase, payment, safety controls, communication, and other means. The most widely used technologies in this field are the barcode and the smartcard scanning. Among all other available solutions, RFID systems (Radio Frequency Identification) have three major advantages: identification is passive, contactless, and reconfigurable. Like smart cards, data is stored on an electronic data-carrying device, called the chip. However, RFID devices do not require physical contact between the chip and the reader. Instead, data is exchanged with an electromagnetic field. Electromagnetic waves are emitted and received through two coils, or antennas. One is connected to the chip and the other one in the reader. The chip, when accompanied by the coil, is called the transponder.

To maximize the power transmission, and the working distance between the transponder and the reader, the resonant frequency of the system is used to convey information. Two types of transponders exist today: passive and active transponders. A passive transponder does not provide energy and, instead, receives it from the reader's magnetic field. This energy causes an impedance change of the transponder: shifting the initial natural frequency of the system, which is detected by the reader. Active transponders carry a battery that allows them to transmit their ID signal using their own

energy source. The signal is sent either periodically or in the presence of an RFID reader. Passive transponders are more widely used because they are less expensive, whereas active transponders are used in long distance applications [5].

3.4.2 Wireless Power

Wireless energy transfer is as old as alternating current [7]. The transformers that are ubiquitous in most electronic devices and indeed in all electricity distribution network transfer energy by using mutual inductance. In recent years wireless energy transfer for an array of application is quickly becoming an important use of resonant inductive coupling. A team of MIT physicists, and many others have been working on this subject [8][9]. They realized that resonant objects tend to couple, as opposed to off-resonant interaction, where their interaction remains extremely weak. Thus, energy transfer efficiency between two resonators increases based on the coupling level between them. This phenomenon is called non-radiative wireless energy transfer. Non-radiative energy transfer is much more interesting than other solutions, such as radiative transfer or directed radiation modes because, respectively, they produce a huge energy loss or require line of sight between transmitter and receiver. Some foreseen applications for non-radiative wireless energy are:

- Charging portable electronic devices by placing it within the source field
- Supplying power to mobile robots and machines in a factory
- Supplying power to internal medical device (pacemaker, medicine delivering devices, etc.)

Several designs have been tested and refined. Currently, the highest efficiency is achieved with a four-coil apparatus: the power supply with an inductor, first resonator, second resonator, and the receiver with the device to power (light bulb). A schematic of the system is given in Figure 9.

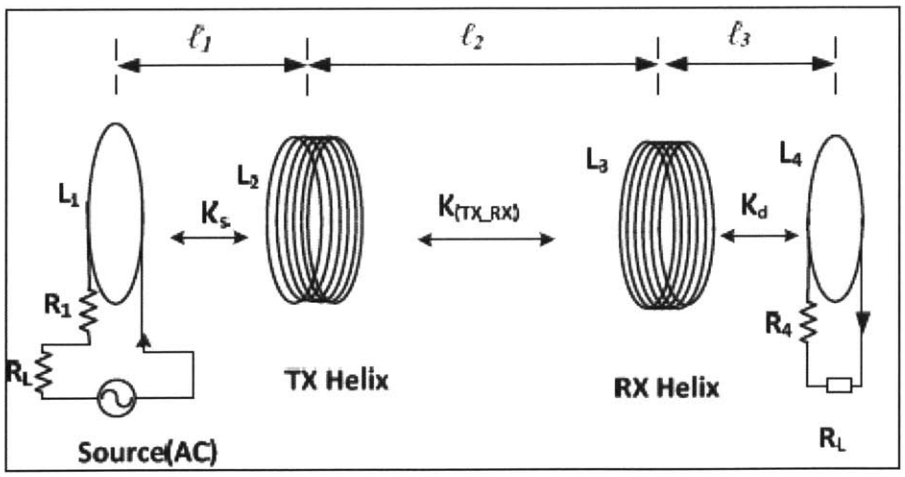

Figure 9: Typical strongly coupled magnetic resonance (SCMR) system. TX is the transmitting helix. RX is the receiving helix. [10]

In this configuration resonant inductive coupling only takes place between the two resonators. The transmitting helix is inductively coupled with the source loop. Similarly, the receiving helix is inductively coupled with the load loop. With this system, several promising achievements have been made including more than 90% efficiency at 15 cm distance, 40% efficiency with a single receiver at 2 m, and 60% efficiency with multiple receivers at 2 m. Recently, the research team, now an MIT spin-off company called Witricity, introduced a repeater to further increase the effective distance of the magnetic field, and thus increase the transfer distance even further by inserting another set of resonators between the two previous ones (transmitting and receiving helixes). Ultimately, the work done at MIT is similar to our project, in that we want to extend the range of a magnetic field via resonant coupling. [9] [10] [11].

Chapter 4

LC Circuit Manufacturing

ProTeqt had previously determined that an LC circuit with a resonant frequency near 220 kHz would be necessary for distance activation. This circuit would be part of each device, and therefore must be compact enough to fit in the locking device and inexpensive enough to keep the device cost low. These requirements make the design and manufacture of this circuit critical to the success of this product. In this chapter we examine a variety of methods for making such a device.

4.1 Introduction to the LC Circuit

As mentioned in the previous chapter, there have been many experiments and tests in the wireless energy transfer design space. ProTeqt had done preliminary research to explore the design space, and found that the performance achieved by the LC circuit could prove feasible for extending the working distance of their locks to one inch. The LC Circuit can be thought of as a passive receiver. That is, the LC circuit does not contain a battery or any other power source, nor does it require its own power source to receive a signal. LC circuits can be manufactured at a very low cost because they do not contain a power source.

An LC circuit only contains an inductor (L) and a capacitor (C). Thus, manufacturing is rudimentary. One must simply join an inductor and capacitor to complete the circuit. Based on the inductance and capacitance of the two components, the natural frequency of the circuit can be predicted with the following equation:

$$f = \frac{1}{2\pi\sqrt{LC}} \tag{4.1}$$

This leaves two variables that can be changed with respect to each other, in order to achieve a certain natural frequency. The most efficient transfer of wireless energy occurs when the transmitter, or deactivation tablet, emits an electromagnetic field at the natural frequency of the LC circuit. It's here that ProTeqt would like to be in the design space.

4.2 Inductor Manufacturing

An inductor, in its simplest form is a coil of wire used to resist an electrical current change [12]. A conductor resists motion of an electrical charge; an inductor resists current flow based on self inductance. The coil of wire stores energy in a magnetic field created by current flowing through a coil. Inductors come in many shapes and sizes. These parameters often affect inductor performance [13]. The magnetic field created by an inductor is dependent on inductor shape, whereas the intensity of the field is determined by the number of turns within the coil. For our application we are interested in designs that will permit an electromagnetic field extension through resonant coupling. Materials are especially important in inductors. The time required to establish a magnetic field is proportional to the coil resistance [12]. High current is desirable to quickly set up a magnetic field. Changing the linear length of the coil, or the coil's material properties can alter resistance, and therefore the field [13]. High coil resistance will also result in heating, and therefore promotes energy loss.

For this project, three inductor-manufacturing methods were analyzed: chemical etching, coil winding and screen printing. After consulting ProTeqt's manufacturing partner, MeadWestVaco, winding is currently the cheapest method to make coils quickly and in a repeatable fashion. However, other methods may be considered for two reasons:

- If they can achieve better energy transmission between the primary and secondary coils, or
- If they become more competitive in the near future.

4.2.1 Chemical Etching

Chemical etching is a controlled material removal process that uses a resist to prevent portions of a material from being removed by a chemical etchant. Once the resist is removed, a desired pattern remains (Figure 10). The process at hand uses copper and a resist to etch a copper pattern.

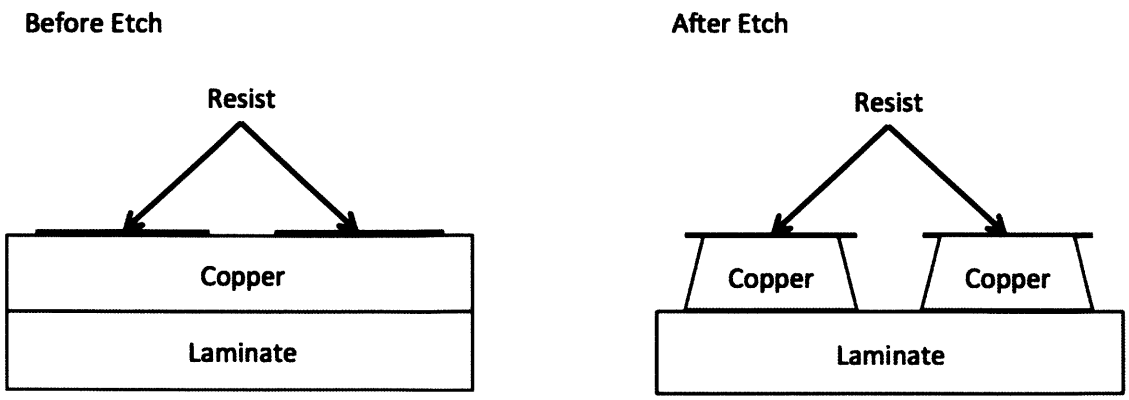

Figure 10: Schematic of a typical etching process.

Figure 10 explains how chemical etching works [14]. You will notice that the etchant removes material in two directions, not just vertically. That is, a slight angle is apparent in the final product because the etchant is in contact with that portion of the material after it passes beyond the resist. Finally, it's important to not that this is a chemical material removal process. Meaning the copper that is removed cannot be easily recycled, making the process as a whole, inefficient.

Etching allows for batch processing of inductors however, it restricts coil designs to single layer, flat spiral coils. Economical etching is usually done in large batches of very thin materials. These materials are often on the order of 0.03mm thick [14]. As material thickness increases, time to etch increases. This property is inefficient in terms of processing energy. This directly impacts the production cost.

As material thickness decreases, resistance increases. This resistance restricts current flow through the material, and therefore increases the amount of voltage needed to create an electromagnetic field. The time requirement to etch thick pieces of copper (0.5mm) is about 5 minutes [15]. This however is not what limits the chemical etching process in terms of this application. The limiting factor is in the material costs. Copper is very expensive, and is only one of the materials used in the process. Resist and the chemical etchant also need to be purchased, along with the many cleaning solutions used to remove the etchant.

4.2.2 Coil Winding

Coil winding is a process that bends a wire (usually radially) into a desired shape. This can be done manually or automatically, and many different winding patterns can be achieved. This process bodes well for inductor manufacturing because an inductor, in its most basic form, is a wound coil. Size and shape of the coil, and wire used to create the coil can impact the inductor performance. Wound coils can be formed into almost any desired shape including flat spiral, cylindrical, rectangular, etc. Wire geometry is often limited by market availability. Rectangular and circular cross sectional wire are most common. Wires are found most commonly in certain AWG gage sizes, which have a circular cross section. Diameters are fully customizable depending on the type of winding machine. Usually machines can operate using a range of wires. Automatic machines often integrate several functions including dispensing, winding, and cutting the wire. Machines can accommodate simultaneous coil winding, providing a batch process. Batch processing allows the machines to produce coils at a high rate.

The cost of wire is extremely cheap [16]. Wire is packaged as a large spool that is fed into the coil winding machine. Because the wire is continuous, there is almost no waste and the two ends of each coil are left exposed, ready to be soldered to the remaining capacitor.

4.3 Capacitors

Capacitors are common electrical components used in many types of circuits. They consist of two conductive plates that are separated by a dielectric layer. This configuration allows capacitors to hold a charge. Capacitors come in many shapes and sizes for different applications (Figure 11). Capacitors are made in extremely high volumes by expert manufactures. With their cost at $0.0074 / capacitor[2], ProTeqt will be purchasing capacitors to use within their circuit.

[2] Fenghua part number 0805CG9R0C500NT, quantity 10,000

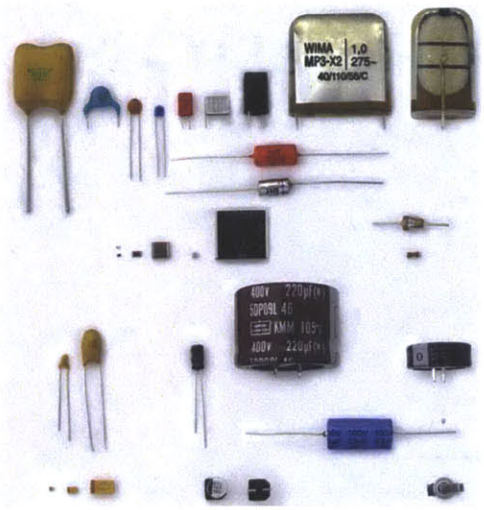

Figure 11: Typical shapes and sizes of capacitors.

Capacitor specifications usually include three key pieces of information: nominal capacitance and rated voltage. A capacitor will likely have these values printed on its side. A capacitor reading 1 μf 20% at 100V, for example, will have a nominal capacitance of 1 microfarad with a tolerance of ± 20% (0.8μf – 1.2μf). Throughout the life of the capacitor, it should not handle more than 100 volts, as that is the rated voltage.

4.4 Soldering Techniques

Soldering is a method of joining two thin metals using a filler material. This filler material has a lower melting temperature than the two thin metal pieces, allowing the filler material to flow between, and bond to each of the thin metal pieces. The filler material is often made of tin and lead. Conductive properties allow soldering techniques to be prevalent in the electronics manufacturing industry, and especially circuit board manufacturing. Two common soldering methods are used in manufacturing today: robotic soldering and dip soldering.

Robotic soldering often uses a robot or other automation to control temperature and the feed rate of the filler material. Sophisticated control systems are used to gain a high level of precision over soldering processes. Robotic soldering often requires auxiliary tooling or methods of positioning and orienting components before they can be soldered.

Dip soldering is used more extensively for circuit board manufacturing. This process is used to solder several components simultaneously. Leads from electrical components protrude through the bottom of the printed circuit board. These are dipped into a lead-tin bath, where the solder then solidifies upon removal. [17]

4.5 Screen Printing

Screen printing is a highly integrated manufacturing process that can provide an entire LC circuit in one process. This means that it can produce the inductor and the capacitor in one process. The process uses a mask that contains the circuit pattern. Conductive ink is then deposited on the mask, and the circuit is printed on the areas not protected. Silver and Aluminum are the most popular conductive inks used in this process. Dielectric materials can also be used to print capacitors. This is done in layers. First a silver layer is deposited, followed by a dielectric, and finally another silver layer. [18]

The flexibility of screen printing is similar to that of chemical etching. It is commonly used for making flat, flexible circuits. The deposited layers are very thin (40 micron), but can be built up in layers. Building layers requires more processing time, and is therefore less economical. The thin nature of screen printing causes inherently high resistance values. Capacitors are printed as large flat surfaces, requiring a large amount of surface area. Spacing is also critical in screen printing. The silver ink does not have an insulating coating, so line spacing also requires more space. Like chemical etching, large batches can be printed at once. However, screen printing requires no post processing because the capacitor can be printed as part of the circuit. [18]

The screen printing process is relatively new when compared to processes like etching or winding. While the added flexibility and integrated components are great for circuit board design and manufacture, it is still a new processes, and therefore costly. Even at the materials level, silver inks are much more expensive than copper for a given volume. While this process isn't right at this time, future developments could lead to significant cost reduction, leaving it as a potential process for future manufacturing. [18]

4.6 Manufacturing Recommendations

As stated above, three manufacturing methods; winding, etching and screen printing were chosen to conduct a preliminary comparison. The manufacturing analysis is based on three criteria: design feasibility, cost, and manufacturing feasibility. For more information on this topic, please refer to Tianyu Zhu's thesis [19].

Engineers at ProTeqt had been successful using a hand made wound coil. The coil was made of AWG 24 copper magnet wire, with 9 turns. It had an oval shape to maximize its surface area. The hand wound coil was created to mimic the coil shown in Figure 12.

Among the three potential manufacturing methods, winding is the most straight forward, and cost effective. Being that the existing coil was hand wound, there is a high variability associated with the manufacturing method. Producing wound coils of the same dimensions by machines would prove to be more repeatable, especially in terms of inductance. The length of wire would be very consistent, providing a repeatable resistance in the copper wire. For etching and screen printing, however, the resistance of the coil is significantly higher due to the very thin nature of the processes. Metal foil used in etching is normally thinner than 0.1mm. Thicker foil will increase cost and the manufacturing time. The thickness of a screen printing pattern is normally below 100μm. Multiple-layers are feasible, but just as with increasing the thickness of foil in etching, it will raise both cost and process time.

In addition to the design challenge, the manufacturing cost of etching and screen printing is higher than winding. Etching, being a fairly complicated process, requires higher equipment cost, includes a complex procedure, and has more material waste than winding. For screen printing, the cost of ink alone is higher than $0.05. Taking all the factors into consideration, winding was the manufacturing process chosen to perform future design optimization and analysis. Again, for a more detailed manufacturing cost analysis and further information on the decision to use wound coils, please refer to Tianyu's thesis [19].

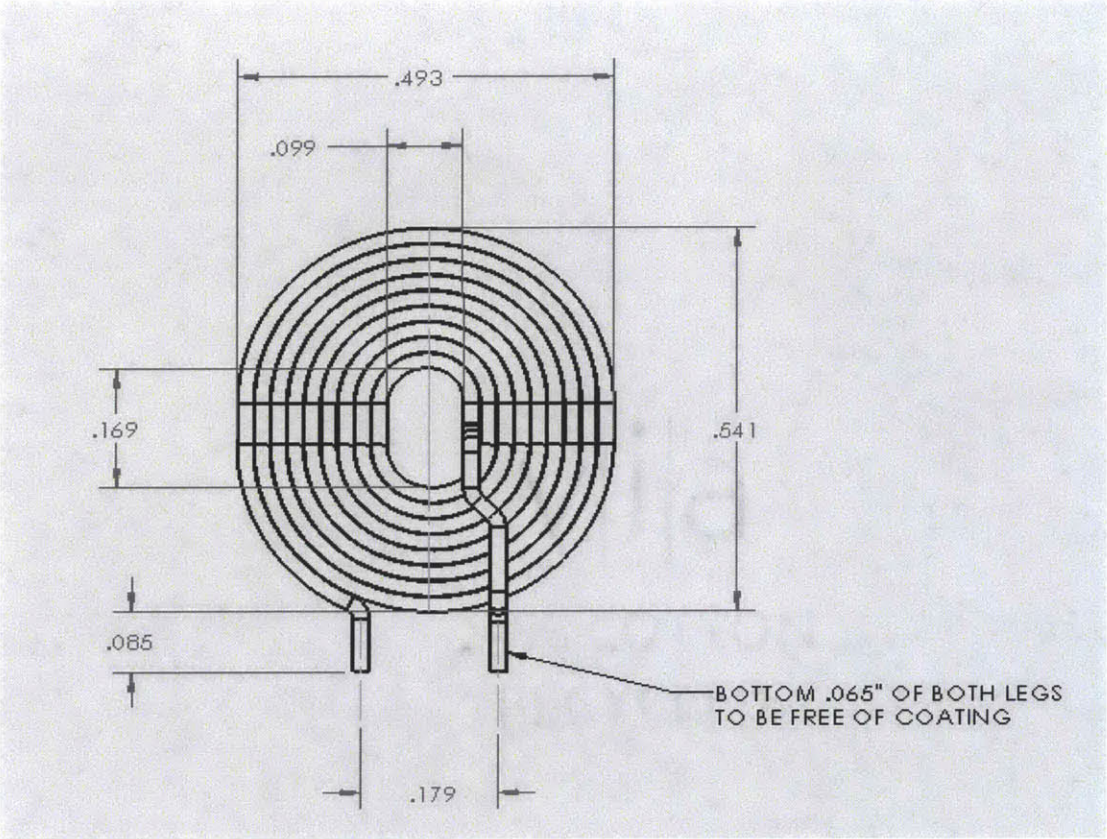

Figure 12: Example of a hand wound coil design.

Chapter 5

Coil and Circuit Design

5.1 Objectives and Design Constraints

The objective of this section is to provide an optimized design of the LC circuit after understanding all of the constraints, whether set by ProTeqt or inherent in the manufacturing process of the coil. For a more detailed analysis of coil design please see Amaury Rony's thesis [20].

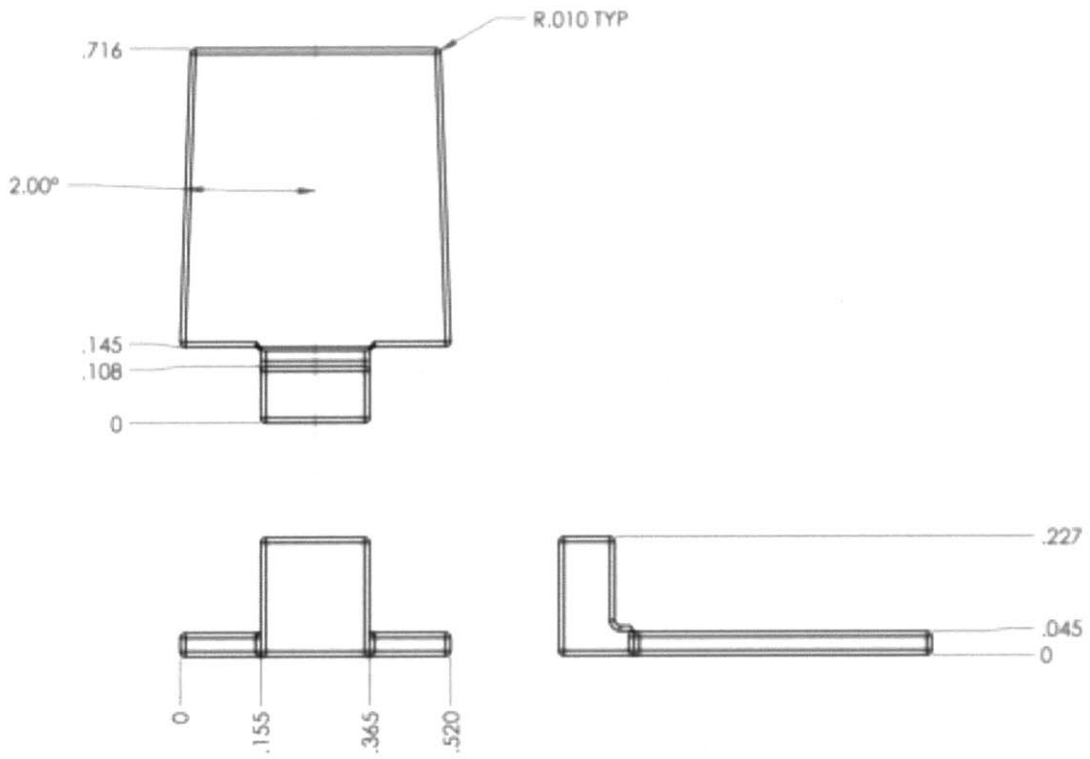

Figure 13: Usable volume (in inches) inside the lock, dedicated for the LC circuit.

As previously discussed the LC circuit at hand will be designed as a passive receiver that will extend ProTeqt's unlocking capabilities to one inch above the tablet. The two components of the circuit are the inductor and capacitor of, which, the inductor provides the most freedom in terms of design. The circuit design must consider several constraints. First, the circuit must comply with the existing design for the micro USB

lock. ProTeqt has designed the external housing with an opening in which the circuit must fit. This introduces geometric constraints. The circuit must not exceed a diameter of 12.74 mm, and should be less than 1.143 mm in height (see Figure 13). Other constraints include functionality at an inch above the surface of the tablet and manufacturing cost at less than $0.05.

5.2 LC Circuit Experimentation

The inductor and capacitor share a relationship that can be optimized in order to create the most effective field, thereby heating and expanding the enabler. The most important design component is the inductor because it must act as an antenna and generate it own field. The inductance depends on the geometry of the coil. the wire gage size and number of turns in the coil. Once the inductor has been optimized in terms of gage size and turns, a capacitor can be chosen to target a certain natural frequency for the circuit.

To find the optimal inductor geometry a design of experiments was conducted to generate a response surface based on the wire gage and number of turns in the coil. The measured output of this test was voltage, which was converted to current based on the known resistance of the coils. To conduct the experiment a primary coil was connected to a function generator and amplifier and placed below a surface representing the deactivation tablet. Above this setup, six different circuits with different inductor geometries were connected to an oscilloscope in order to measure the peak-to-peak voltage. From here the values were converted into current using the known resistance and inductance values of the coils To maximize the field generated by the inductor, the current in the coil should be maximized. This will create a strong magnetic field, providing the maximum amount of eddy currents used to generate heat in the enabler.

The deactivation tablet has been optimized to operate around 220 kHz. To operate around this natural frequency we measured the inductance of each coil, and then paired it with the proper capacitor. After generating the response surface, the inductor geometry was optimized based on the geometric lock constraints. The capacitor was then selected based on the optimal geometry. The pairing of the two components lead to the optimal design of the LC circuit.

Using the optimal design, experiments were conducted to understand the coupling efficiency between the two coils. To measure the efficiency, voltage was measured in the primary circuit, and the LC circuit. The ratio of voltage measured in the LC circuit to the voltage measured in the primary coil was recorded with respect to frequency. Finally, using this method, the effects of placing the circuit inside the lock were analyzed to understand the effect of the lock on the efficiency of the coupling between the primary coil and the LC circuit.

5.3 LC Circuit Optimization and Test Results

The inductor and capacitor share a relationship that can be optimized for the most effective field, thereby heating and expanding the enabler. The most important design component is the inductor because it must act as an antenna and generate its own field. The inductance depends on the geometry of the coil. The inductance will change with the wire diameter and number of turns, especially considering that we are making flat spiral coils: as the number of turns increases, the diameter of the coil as a whole increases, therefore allowing it to intersect with more lines of flux from the primary coil.
As we tested our six coils of varying gage size and number of turns, we gathered data and generated a response surface that would help us to predict the performance of any other combination of gage sizes or number of turns. The response surface can be found in Figure 14. From this surface we see that the wire gage and number of turns in the coil should be maximized to generate the most current. Intuitively we would want a larger gage size to reduce the resistance and thereby increase the current. Also, increasing the wire gage corresponds to a shorter wire. If we had two coils that had the same outer diameter, but different gage sizes, the larger gage size would have a shorter unwound wire, which again decreases resistance and increases current flow.

With a general understanding of how current corresponds to a coil design, other constraints were considered in order to fully optimize the circuit. It was found that the largest gage size that could fit within the given allowable volume of the lock was AWG 24. This wire diameter is around 0.5 mm. This is the maximum gage size because the wire must be routed in and out of the flat spiral coil, making the coil thickness at least twice the wire diameter, effectively requiring us to cut the allowable height in half. With

the wire gage in place, we calculated the maximum number of turns that would fit in the cavity to be 9, when leaving an appropriate inside diameter for the manufacturing of the coils. A theoretical model was created to confirm this design. Table 1 shows the optimal coil using the theoretical model. The output of the model is current. For more on the theoretical model, please see Amaury Rony's thesis [20]. From the table we again gather that optimal design for the inductor coil uses 24 AWG wire for a coil with 9 turns.

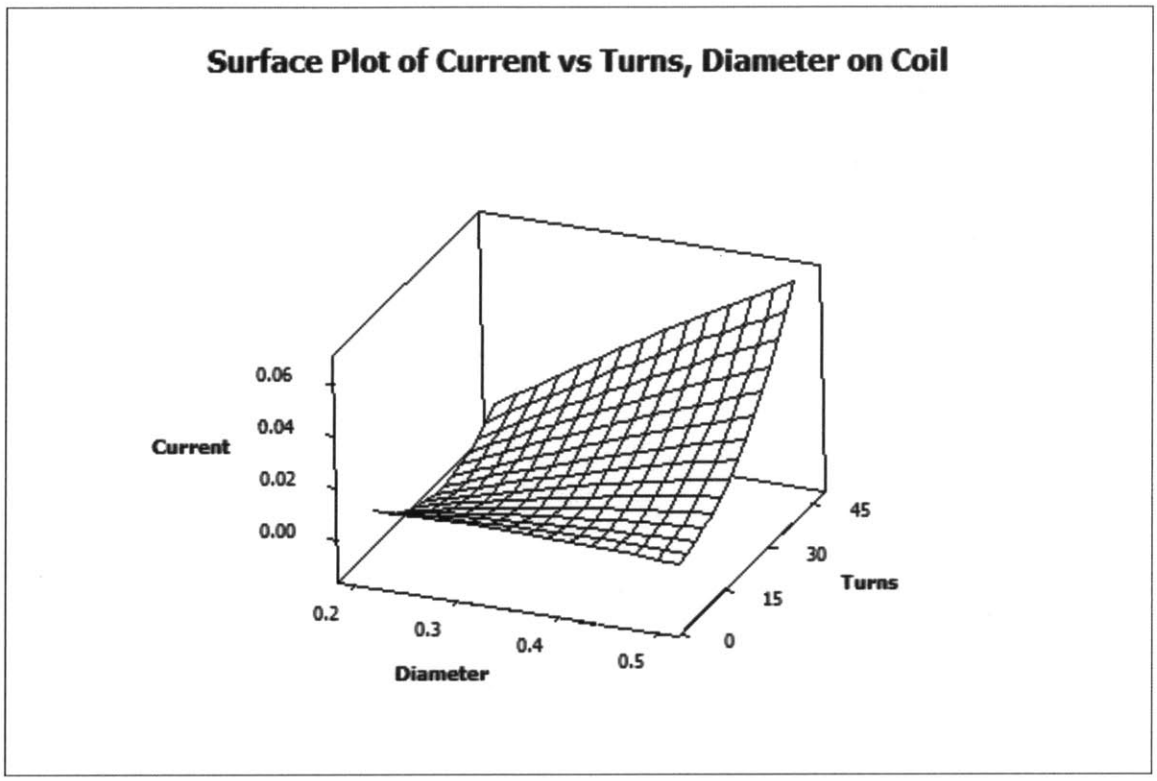

Figure 14: Response surface in current for various coil characteristics.

AWG \ Turns	6	7	8	9	10	11	12	13
22	4.76	5.29	5.82	6.36	6.90	7.45	7.99	8.54
23	3.56	3.94	4.31	4.69	5.07	5.45	5.83	6.21
24	2.68	2.94	3.20	3.47	3.73	4.00	4.27	4.54
25	2.03	2.21	2.39	2.58	2.76	2.95	3.14	3.33
26	1.53	1.66	1.78	1.91	2.04	2.17	2.30	2.43
27	1.17	1.26	1.35	1.44	1.54	1.63	1.72	1.81
28	0.89	0.95	1.01	1.07	1.14	1.20	1.27	1.33

Table 1: Circuit design optimization with gage size (left) and number of turns (top). The current is recorded for each pairing of gage size and number of turns. The optimal value can be found at AWG 24 and 9 turns. Grey cells are not feasible solutions due to volumetric constraints.

Moving forward, a capacitor needed to be joined to the coil to complete the LC circuit. The capacitance was calculated using the natural frequency of an LC circuit, which is given by:

$$C = \frac{1}{(2\pi * f)^2 * L} \qquad (5.1)$$

. With the tablet being optimized to operate around 220 kHz, we could easily back calculate a capacitance value for the inductor so that the natural frequency of the LC circuit would be 220 kHz. A 1 microfarad capacitor was included in the final specifications for the circuit, because it's the most common capacitance value near the theoretical value calculated using the formula.

With the final specifications of the circuit design in place, the circuit was analyzed to understand the coupling efficiency. Using the methods discussed above, we were able to obtain plots of the ratio of current in the secondary coil to the current in the primary coil (which we define as efficiency), as a function of frequency. Figure 15 shows a typical plot.

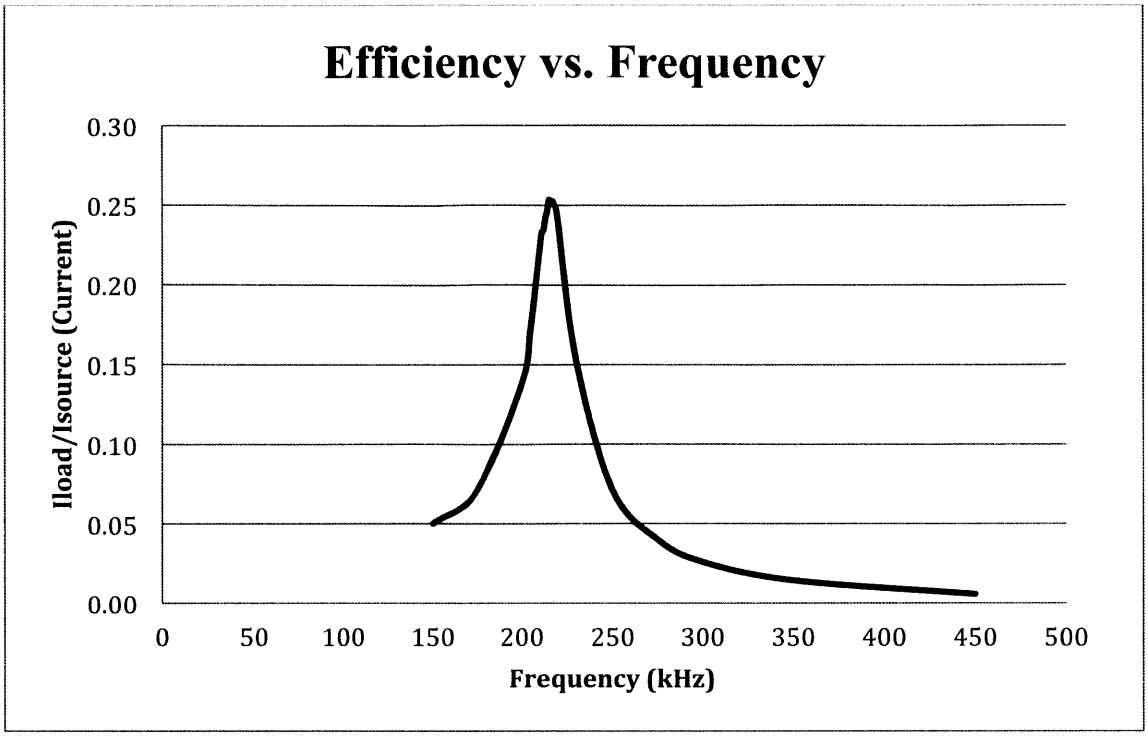

Figure 15: Efficiency vs. Frequency plot for an LC circuit. Efficiency is defined as Iload / Isource or the current in the circuit over the current in the primary coil.

Notice the large spike in efficiency around 220 kHz. This is the frequency that the primary coil uses to emit its field, and that the LC circuit is tuned to. It is at this frequency that the two are resonantly coupled and have the highest effective wireless energy transfer.

Naturally the next step was to test the circuit to understand the effects of the other metal components in the lock. The fear was that other conductive materials inside the lock could shift the natural frequency of the circuit if within a close proximity. It was found that the enabler had an extreme damping effect on the coupling efficiency of the circuit. This meant that, we were able to expand the enabler with less energy transfer than expected. Figure 16 is a plot comparing the efficiency of the LC circuit with and without the enabler.

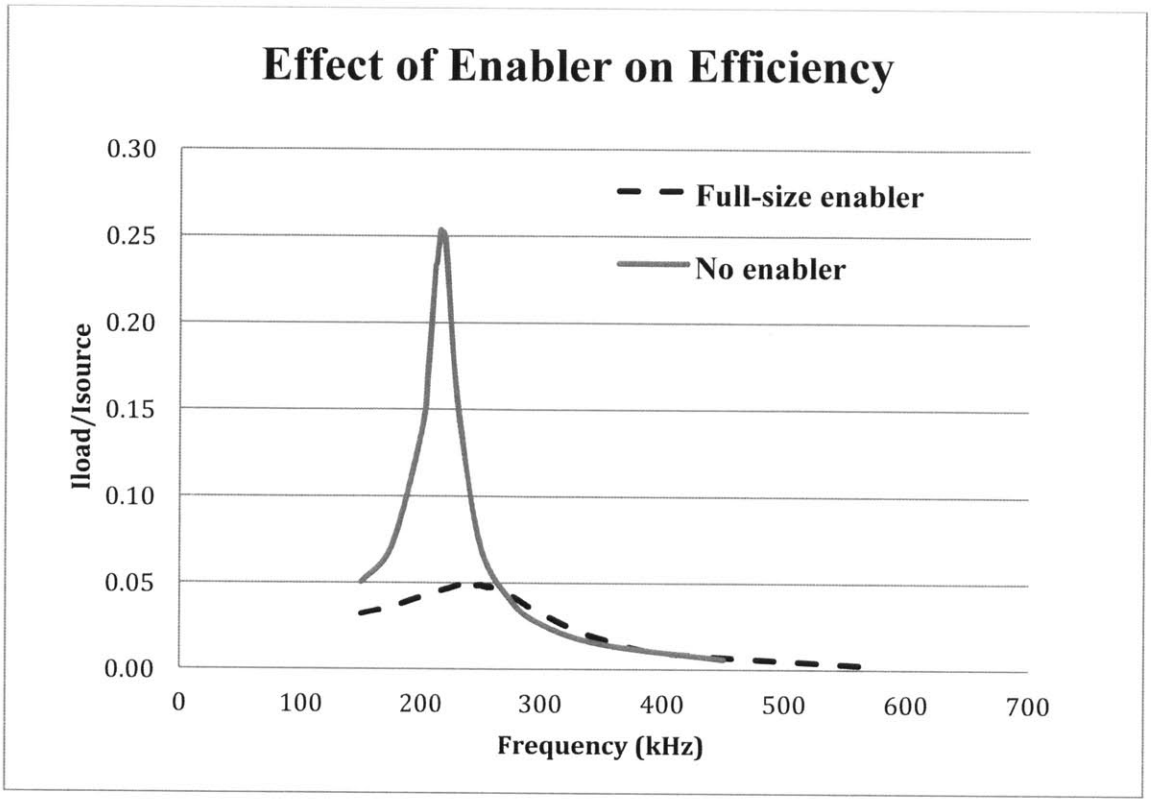

Figure 16: Efficiency vs. Frequency plot for an LC circuit with and without a full sized enabler.

It's evident that the enabler dampens the efficiency of the wireless energy transfer by about five times. To further understand the effects, a half sized enabler was analyzed using the same method. Here it was found that the efficiency was still damped, however the extent was significantly less. This effect can be seen in Figure 17.

The final conclusion from the circuit design modeling and testing was that the optimal coil design was empirically feasible for the application at one inch. For more information about the testing and the approach to the conclusion see Amaury Rony's thesis [20]. However, moving forward ProTeqt was interested in how well their lock would perform at an inch, and whether or not the insight about the half sized enabler would be beneficial in their future designs.

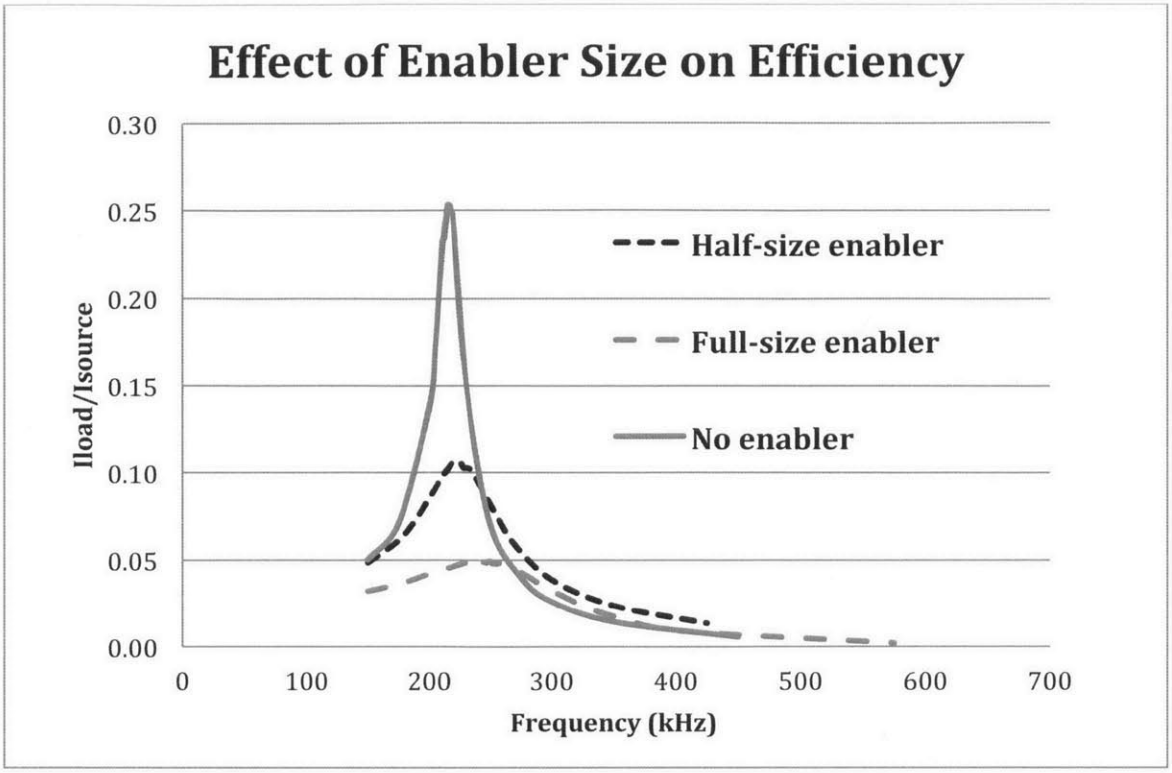

Figure 17: Efficiency vs. Frequency plot for an LC circuit with and without a full and half sized enabler.

Chapter 6

Mechanical Lock Analysis

6.1 Objective

The success of ProTeqt requires the force generated by the enabler to be greater than the force required to disengage the mechanical system. The objective of the analysis on the mechanical lock can be separated into two parts. First understand the forces required to disengage the lock should be understood, followed by the forces that can be achieved by the enabler at a distance of zero and one inch. As mentioned in the previous chapter, ProTeqt is not only interested in the performance of the original enabler, they are now interested in understanding the performance and capabilities of using a half sized enabler to increase the wireless power transfer between the primary coil and the LC circuit.

6.2 Mechanical Lock Force Analysis Methodology

To better understand the forces required by the lock to disengage, three analyses were completed: finite element analysis (FEA), analytical calculations, and empirical data collection. By completing a thorough analysis of the forces required to disengage the lock, ProTeqt will, for the first time, understand the performance of their current lock design, and be better prepared for future designs.

6.2.1 Finite Element Analysis (FEA)

In order to fully understand the interactions and forces required inside the lock, an FEA was conducted to gather baseline intuition on the bending required before disengagement. The FEA was completed using 3D data for the most current lock design. Solidworks Cosmos was used to conduct the analysis.

Looking at the schematic of the lock (Figure 18), force is applied to the first sheet metal piece from the enabler through other internal components not shown. For the scope of the FEA, and the breadth of information we wished to obtain, we simplified the

model, focusing on the force required to bend the sheet metal component. An image of the full component can be found in Figure 19.

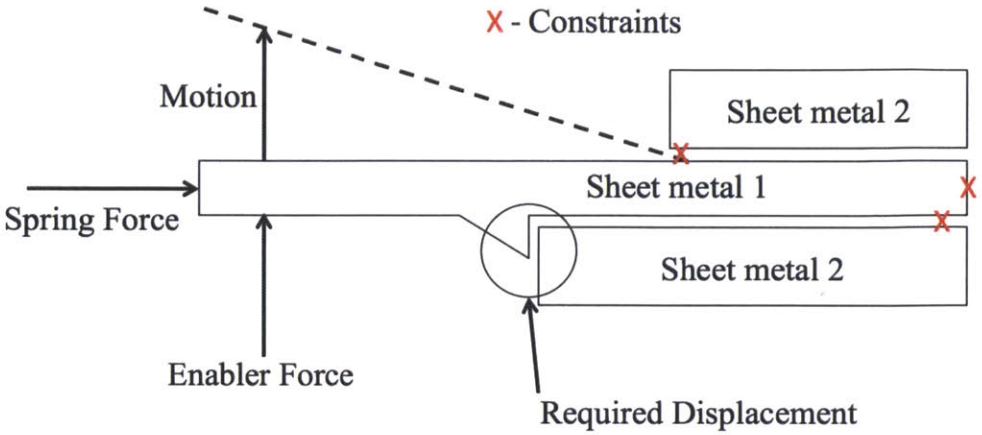

Figure 18: The interface between the two sheet metal components including constraints, forces, and resulting motion.

The majority of this component is housed inside of the other sheet metal component. As stated before, the second component acts as a sheath for the component above. The tab that is protruding in the image above contacts the inside surface of the sheath. It's here that we must constrain the FEA model from the top. Secondly, the model is constrained from underneath at the point which it again contacts the sheath. ProTeqt made decisions related to material selection. Ultimately, stainless steel was used for both sheet metal parts. Figure 19 better describes the interface between the two parts including the movement and visual of the required displacement.

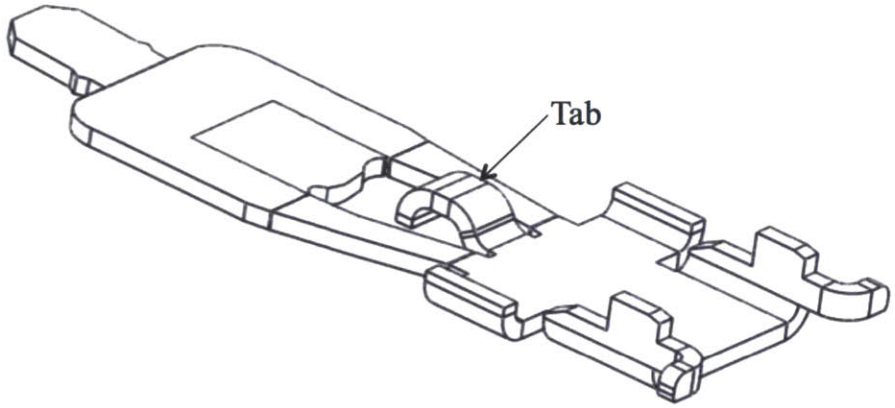

Figure 19: Image of the first sheet metal component.

To obtain the results of the FEA, we applied varying levels of force until we reached 0.5mm of displacement. At 0.5mm the two pieces clear each other, allowing the first metal piece to be forced through the sheath by the spring. Figure 20 shows the model as prepared for the analysis. A third constraint was added to simulate the product. That is, the product provides a third constraint in the horizontal axis. The small arrows signify points of fixation whereas the larger arrows represent the force.

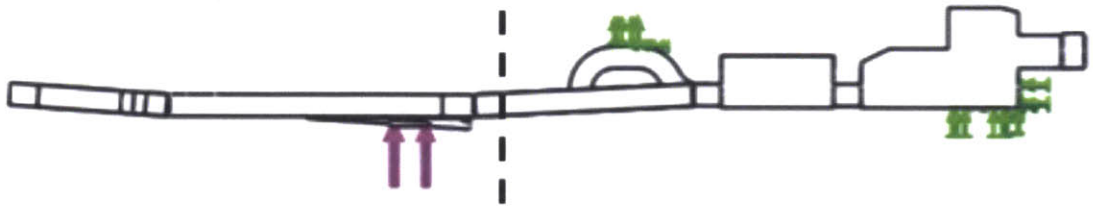

Figure 20: Constraints and loads as applied in the FEA. The vertical constraints are the result of other lock components. The horizontal constraint is a result of the product. The applied load is pink, while the constraints are green. The displacement is measured at the dashed line.

6.2.2 Analytical Calculations

To assist and validate the FEA an analytical calculation was used to further understand the forces required to bend the sheet metal. This analysis used a typical beam-bending model to simulate the forces required by the lock. Overall, the analytical calculations also took frictional forces, as applied by the spring, into account, making it a more robust analysis of the lock. That is:

$$F_{Total} = F_{Friction} + F_{Bending} \tag{6.1}$$

$F_{Friction}$ can be defined as:

$$F_{Friction} = \mu F_{Spring} \tag{6.2}$$

$$F_{Spring} = k(x_0 - x) \tag{6.3}$$

$$k = \frac{Gd^4}{8D^3 n_a} \tag{6.4}$$

$$G = \frac{E}{2(1+v)} \tag{6.5}$$

Where μ is the coefficient of friction between the two stainless steel components, k is the spring rate, x_0 is the free length of the spring, x is the displaced distance of the spring, G is the shear modulus of the spring, d is the diameter of the wire, D is the spring diameter, n_a is the number of turns in the spring, E is young's modulus for the spring material, and v is Poisson's ratio.

$F_{Bending}$ can be defined using the following model:

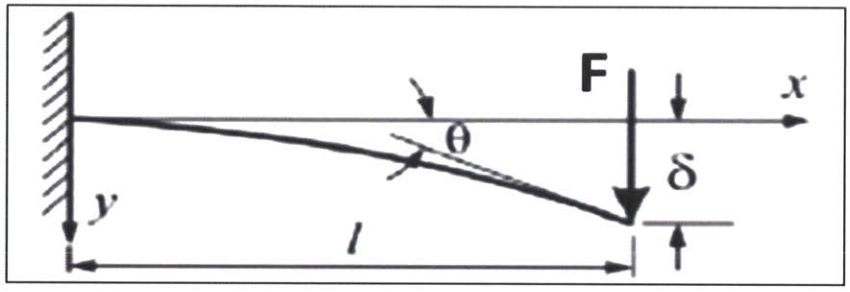

Figure 21: Beam bending model used for analytical calculations.

$$F_{Bending} = \delta(x)\frac{6EI}{x^2(3L-x)} \tag{6.6}$$

Where δ(x) is the displacement at point x, E is Young's modulus of the sheet metal, I is inertia, L is the length of the beam, and x is the position at which the force is applied.

The following tables list the values used to complete the analytical calculations.

Table 2: Values used for the frictional and bending force calculations.

Spring Force						
μ	0.8			Spring properties		
k	5.25E+02	N/m		G	6.90E+10	Pa
x	0.007461	m		E	1.80E+11	Pa
x_0	2.40E-02	m		d	3.60E-04	m
x_0-x	1.65E-02	m		D	2.64E-03	m
				na	15	

Bending Force						
δ	4.34E-04	m		Beam Properties		
x	5.00E-03	m		E	1.80E+11	Pa
				L	5.21E-03	m
				I	1E-14	m^4

Using the values listed above for each parameter in the equation for the frictional component, we have:

$$F_{Spring} = k(x_0 - x),$$

$$F_{Spring} = 8.68N,$$

$$F_{Friction} = \mu 8.68\text{N},$$

The coefficient of friction, μ, is determined by the interface between the two stainless steel parts. We found the coefficient to be 0.8 [21].

$$F_{Friction} = 6.94N$$

Also, we compute the bending component as:

$$F_{Bending} = \delta(x)\frac{6EI}{x^2(3L-x)},$$

$$F_{Bending} = .000434\frac{6 * (1.80\text{E} + 11) * (1\text{E} - 14)}{0.005^2(3 * 0.00521 - 0.005)},$$

$$F_{Bending} = 17.7N$$

In conclusion, we sum the two force components to obtain the total force required to disengage the lock, which is 24.6N for these nominal conditions

6.2.3 Empirical Data Collection

The first two analyses used to simulate the force required to disengage the lock provide an initial level of understanding. However, these analyses are never a perfect representation of the actual force required for any function. This fact requires engineers to be leery about any results obtained by the two types of analyses. To gain a true perspective of the force required, a test procedure was implemented to capture the force required to disengage the lock.

To facilitate testing one side of the external housing was removed, leaving the internal components exposed. The LC circuit, enabler and other internal components were removed for testing. This allowed enough space to access the sheet metal components using a probe fastened the end of a force gage. The spring remained inside the lock throughout testing to provide results that were simulated by the analytical calculations. The measurements are a sum of the forces due to friction and bending.

To facilitate repeatability, the force gage was fixed and set to zero before each test. The lock was then positioned so that the probe on the end of the force gage was directly on the sheet metal. As the lock is brought closer to the force gage the force increases until, finally, the lock disengages. When the lock is disengaged the force drops back to zero. The force gage is able to record the peak force throughout the unlocking process, which is then recorded.

6.3 Enabler Force Analysis

The force required to disengage the lock in turn determines the minimum force required from the enabler. If the force produced by the enabler does not exceed the force required by the lock, it will fail to disengage, creating unhappy customers. The shear number of products that could eventually be facilitated by ProTeqt's technology leaves little to no room for error. The product should never fail to disengage. Accordingly, experiments were conducted to gain a better understanding of the forces produced by the enabler.

6.3.1 Measuring Enabler Force

The experiments were conducted to further understand the interaction and effects of the deactivation tablet and enabler, at a distance of zero, and one inch from the deactivation tablet. The experiments conducted at one inch used the LC circuit to facilitate enabler expansion. The measurement captured by the tests was the force produced by the enabler.

6.3.2 Test Apparatus

With the lock being completely encapsulated a test apparatus had to be constructed that would allow us to reliably measure the force created by the enabler, while maintaining a level of flexibility allowing us to change various parameters. Ultimately, we decided to use a force gage to measure the resulting force after a deactivation cycle. The diagram in Figure 22 explains the setup.

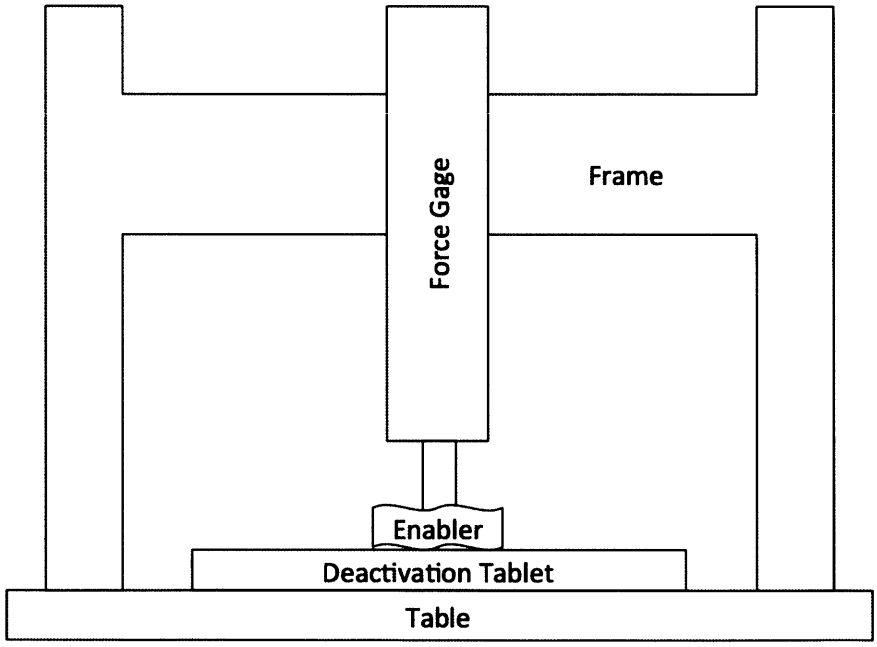

Figure 22: Diagram of the enabler force test apparatus.

The apparatus was designed to comply with the existing design of the deactivation tablet. We built the test fixture on a table that housed the deactivation tablet. On the table, a frame was constructed that allowed a force gage to be repositioned vertically,

over the center of the field produced by the tablet. In the area depicted in the diagram by the enabler, an enabler was placed in a Lexan fixture that was laser cut to certain dimensions required by tests used to constrain the enabler. Another piece of Lexan was placed on top of the constraining fixture. This was placed directly underneath the force gage, while maintaining minimal contact. An example of one of the constraining fixtures is pictured in Figure 23.

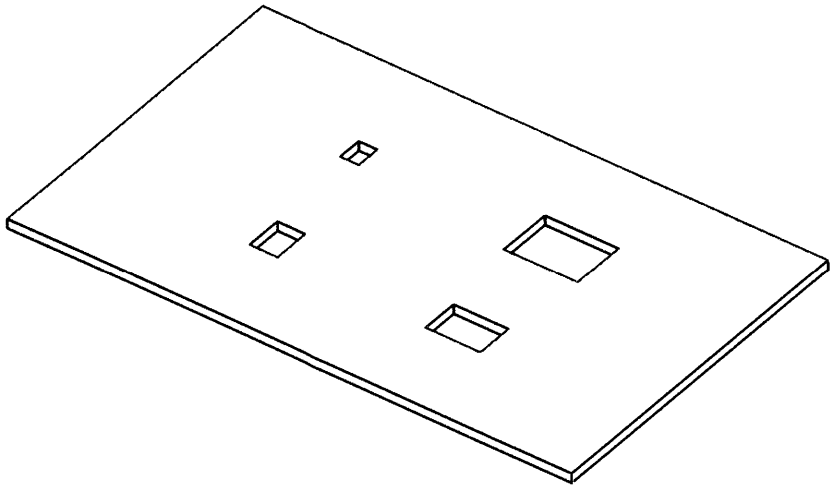

Figure 23: Model of an enabler constraint fixture.

The enabler will fit in one of the pockets. The full size, or current design, is depicted as the largest pocket, and they can be cut down to smaller sizes for testing. The fixture will either sit on a small piece of cardboard directly on the tablet, or on a block that has a height of one inch above the tablet. The cardboard is necessary at minimal distance because the heat generated by the enabler can actually melt the surface of the tablet. This is not the case when used in the lock because the external housing protects the enabler from interacting with the surface of the tablet. The small piece of cardboard also mimics the thickness of the external housing, in that the enabler will never actually be directly on top of the tablet.

As stated earlier, another piece of Lexan is placed over the constraining fixture in a state that minimally contacts the overhead force gage. Upon activation of the tablet, the enabler expands, pressing the second piece of Lexan against the force gage. A peak value is then recorded for each experiment. The force gage used for these tests is less stiff than the beam-bending model used to describe the actions required to disengage the

lock. Therefore, we believe this test apparatus to be a satisfactory design that may slightly underestimate the enabler forces.

6.3.3 Experiments

As stated, a number of tests were conducted to understand the different parameters and components that ultimately lead to the resulting enabler force at zero and one inch. First an analysis of the effects of deactivation time, or time that the deactivation tablet produced the desired field, were conducted to find the optimal time to conduct all proceeding experiments. With a fixed time, the effects of constraining the enabler both vertically, and with respect to its perimeter, were analyzed to predict performance within the lock, given certain dimensional constraints and tolerances inherent in the manufacturing processes.

With an understanding of the constraining effects, tests of the full enabler were run on the tablet and at one inch using the LC circuit. Finally, tests were conducted to understand the effects of using a half sized enabler, as recommended to increase the coupling efficiency between the primary coil and the LC circuit.

6.4 Force Test Results

The analysis and interpretation of the results from the tests explained above will provide ProTeqt with intuition as to the robustness of their current lock design. The analysis can also be used as a future design tool.. In this chapter the results are first presented for the lock, including the bending forces required to disengage the lock using the FEA, analytical calculations, and empirical data collection methods discussed in the previous chapter. The empirical results for the forces produced by the enablers are then discussed. Finally, by combining the disengagement and enabler forces we can predict product failure rates associated with variable enabler performance.

6.4.1 Lock Disengagement, FEA

The finite element analysis (FEA) was used solely to understand the force needed to bend the first sheet metal piece with a displacement of 0.5mm. This is the critical distance as found in the CAD data that will permit the first sheet metal piece to disengage, and slide through the second piece. The results from the FEA are used

primarily to understand the order of magnitude of the force required. After stepping through several iterations of the FEA using different forces, we found that a force of 15N would give us a reasonable amount of displacement at the critical interface between the two sheet metal pieces. The FEA output is a color map of the component. Different colors correlate to the amount of displacement seen at any certain point along the sheet metal. Other iterations for 5, 10, and 15 Newton loads are included in Appendix B.

Interpreting the results of an FEA can be difficult. Rarely will an FEA coincide with the actual force required for any application, since the exact constraints and other conditions are never fully known. In our case, we used the FEA for one analysis. We used hard constraints at each of the three constraining points. This assumes that the interfaces between the sheet metal pieces are perfect, in that dimensionally there is no slop, and that the second sheet metal piece is a perfectly rigid component. In reality, this is not the case. Therefore, the FEA can be used as an extreme maximum for the force required to disengage the lock. Figure 24 is the FEA output for a 15N load.

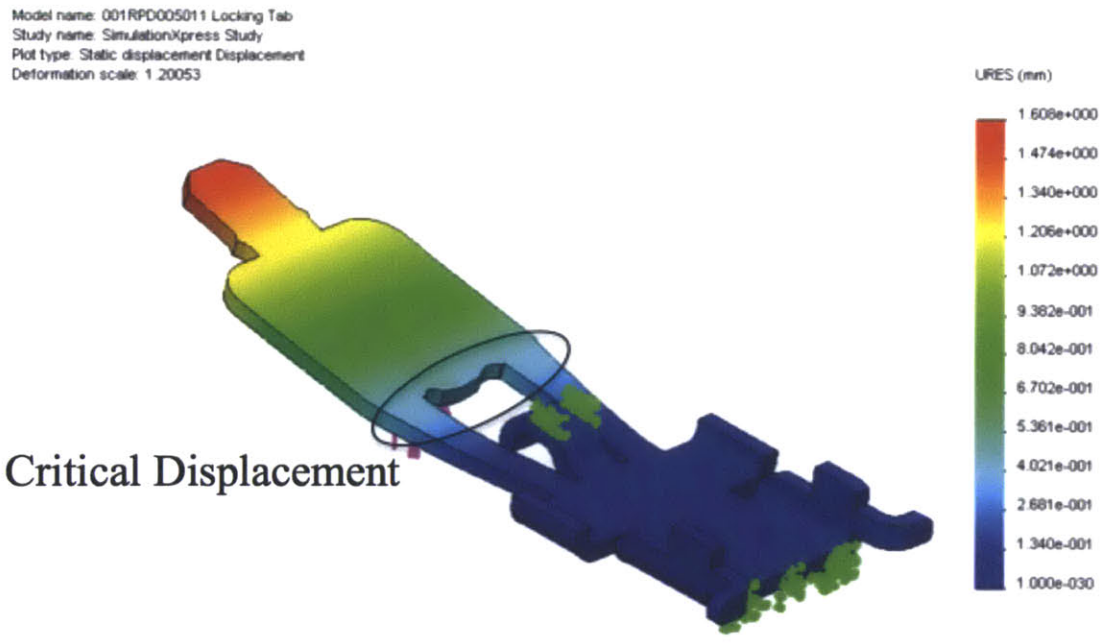

Figure 24: FEA result at 15N. Displacement is measured in millimeters and is color-coded according to the scale on the right.

Using the analytical models listed above, force requirements of 7 and 18N were required for the respective frictional and bending forces. The total force required using this analysis is 25N. This indicates that the FEA model provides a reasonable maximum value for the bending force. More importantly, we confirm the magnitude of the value. This is much more important because, as stated before, many assumptions are built into the FEA model. This is also the case with the analytical calculation.

This analysis, again, assumes that the two sheet metal pieces have zero deviation from their dimensions, thus the components mesh together in a perfect manner. For the calculation of frictional force, the assumption is that the two surfaces that will be sliding past each other are perfectly parallel, making solid contact. In reality this will not be the case. The components are very small, and prone to burrs, inherent in stamped parts. The burrs provide and even smaller interface between the two components, which would lessen the frictional force. These assumptions tell us that, again, the calculations should be used as a tool to understand the extreme maximum values for both the frictional and bending forces.

6.4.2 Lock Disengagement, Empirical Comparison

To get a reliable understanding of the actual force required to disengage the lock, experiments were conducted using the process mentioned above. The force data collected resulted in a mean of 1.84N with a standard deviation of 0.31N. This is significantly lower than the either of the two previous force analyses. Figure 25 shows the distribution plots of the force required to disengage the lock.

To reiterate, the discrepancy between the analytical calculation, FEA, and empirical data could be due to a minimal frictional force, resulting from the manufacturing of the two sheet metal components, and the assumption of dimensionally perfect parts. Realistically, the tolerance between parts in the y-axis can significantly reduce the amount of force required to disengage the lock because the clearance between the two components reduce the amount of displacement that is required to disengage the two sheet metal components. Figure 26 better explains this effect.

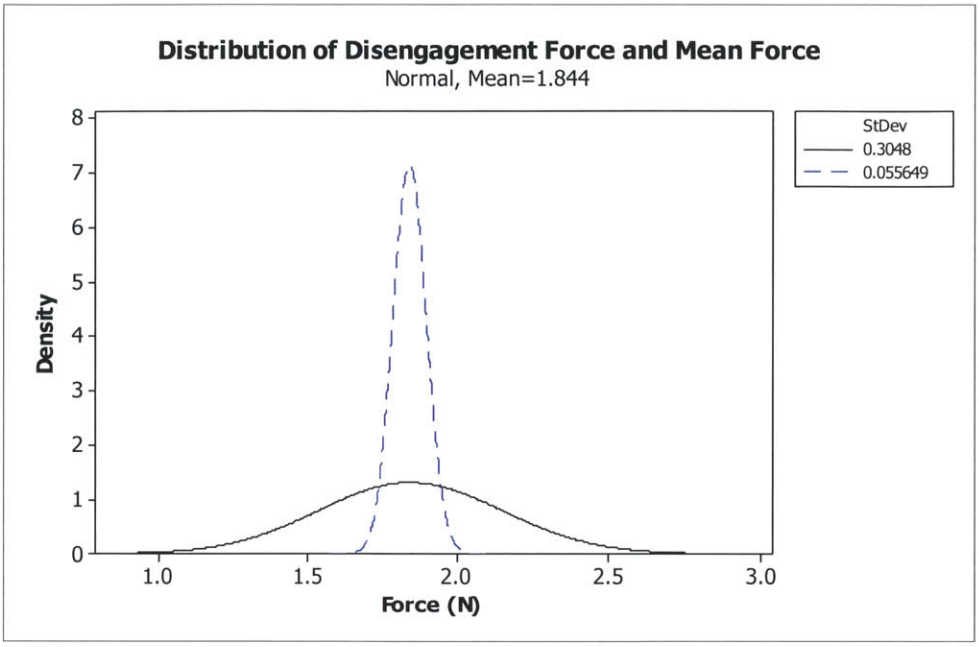

Figure 25: Normal distribution of the disengagement force and the mean force (dashed).

The diagram on the left is a perfect scenario where all dimensions are nominal, and all parts are initially in contact with one another. This is what was modeled using the FEA and analytical calculations. The diagram on the right is a more realistic situation, where x is an initial gap and represents motion that can occur before any bending forces develop. The distance can be subtracted from the required displacement, δ. Therefore the required displacement is now $\delta - x$. Distance is proportional to the amount of force required and a smaller displacement requires a smaller force.

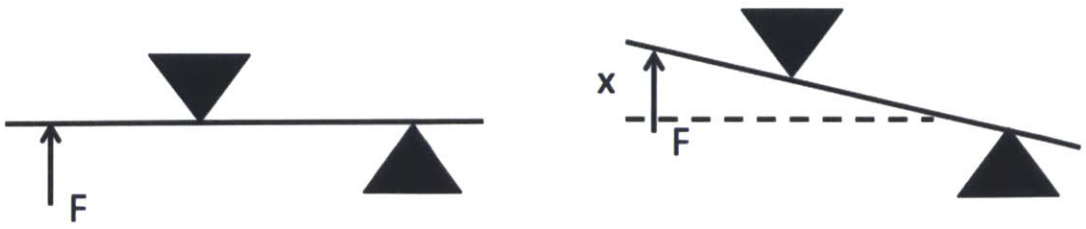

Figure 26: Diagram explaining the effect of clearance in the mechanical lock system. Idealized model on the left. Realistic model to the right.

By running through the analytical calculations using this offset , we find that the total force required to disengage the lock is much closer to the measurements. For this calculation, we let all of the components required for the bending model be the same, except for δ(x). It was estimated that this value could be as low as 0.0001m instead of 0.000434m. The value is merely used to carry out calculations. Accurate measurements of this dimension should be taken in the future. This term is the displacement required for lock disengagement. This change in displacement is reasonable for the amount of play, or available space between the two sheet metal components. Going through the calculations, we now have:

$$F_{Bending} = \delta(x)\frac{6EI}{x^2(3L-x)},$$

$$F_{Bending} = 0.0001\frac{6 * (1.80\text{E} + 11) * (1\text{E} - 14)}{0.005^2(3 * 0.00521 - 0.005)},$$

$$F_{Bending} = 4.07N$$

Letting the frictional component, or spring force, be negligible, or 0N, we find 4.07N to be the theoretical upper limit of the force required to disengage the lock. This theoretical assessment of the force is now only 2.23N away from the empirical results. To reinforce this analysis the FEA model was run using a 4N load, as opposed to the previous 15N load. Now that we are interested in 0.1mm displacement, rather than 0.4mm, it seems the 4N load will suffice.

Regardless, the FEA is about double the measured force required to disengage the lock. We suggest the discrepancy could be due to a few factors that should be further analyzed. First, we were only able to measure one lock, thirty times. This lock was used for months and could have easily been worn from use. While running the tests, we also noticed the impact of the spring. A very long spring is used. When compressed, the spring is not supported and can flex in any direction. This changes the alignment of the spring to positions that could actually reduce the force required to disengage the lock. ProTeqt should consider analyzing the motion in further detail.

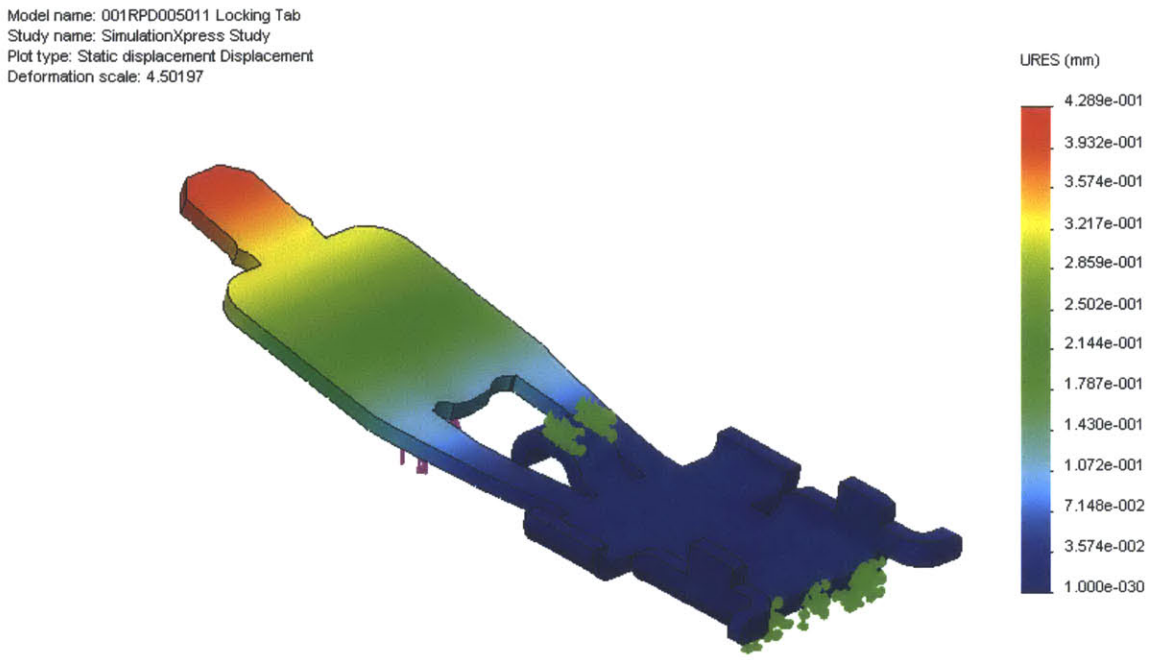

Figure 27: FEA result at 4N. Displacement is measured in millimeters and is color-coded according to the scale on the right.

6.4.3 Enabler Performance

The second component in the mechanical lock system to be analyzed was the enabler. Some preliminary experiments to understand the force generated by the enabler were completed years ago, however the tests were not documented or understood well by ProTeqt. As stated, the force produced by the enabler should be greater than the force required to disengage the lock to ensure reliable performance.

Disengagement of the lock should require less than one second of power from the deactivation tablet. This constraint has been set as per request from ProTeqt's potential customers. To understand the effect of deactivation time on force, five samples were taken at deactivation time intervals (time the tablet is on) of 0.1 seconds from 0.1 to 0.5 seconds. We found that at time greater than 0.5 seconds the enabler burned, producing a negligible force, on the surface of the tablet. After analyzing the data, we decided that operating at 0.2 seconds provided the most reliable results. The data at 0.2 seconds had the lowest coefficient of variation while operating in a range of force that was easily detectable with our instrumentation. In the individual value plot (Figure 28), there appears to be a peak force around 0.3 seconds. This force has a high standard deviation,

which continues to be a trend through 0.4 seconds. While running this test we noticed that just after 0.3 seconds, the enabler would start to burn, mitigating its ability to generate a useful force.

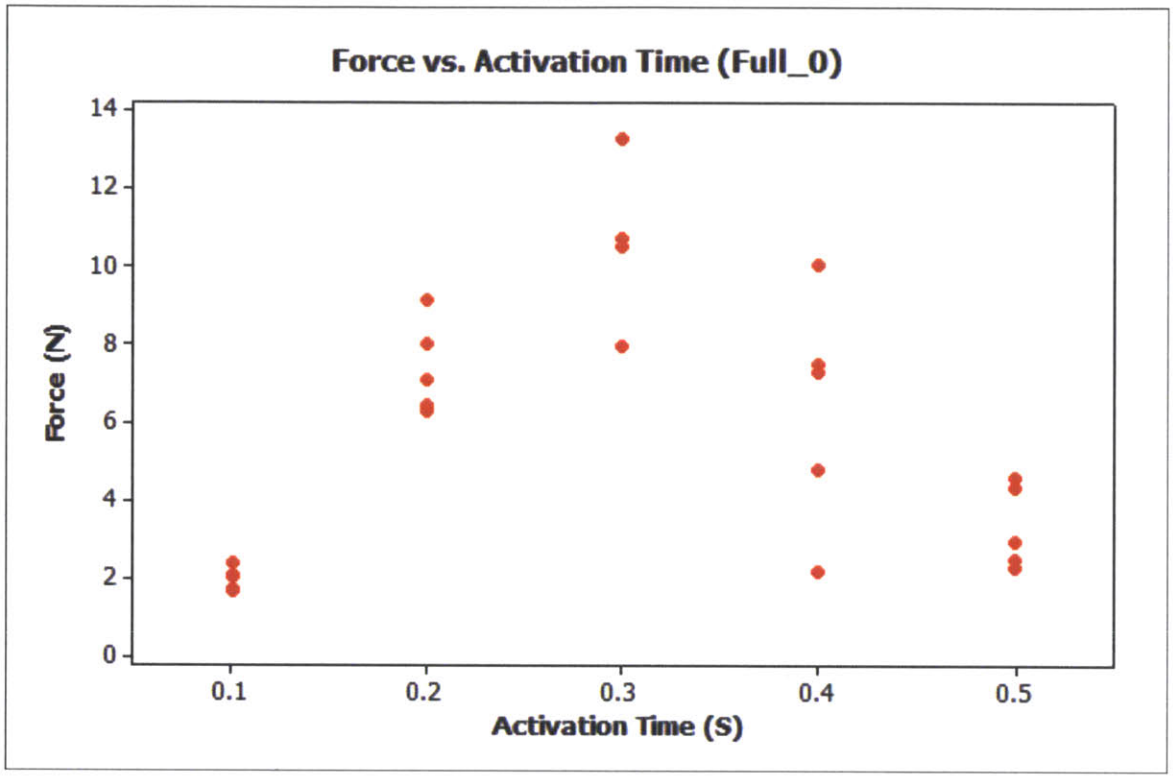

Figure 28: Individual value plot of force vs. activation time using a full enabler on the deactivation tablet

Once the optimal time was established on the tablet, further tests were conducted to measure the effects of constraining the enabler. Cardboard pieces were inserted below the enabler and different sized pockets were cut into the constraining fixtures to help understand these effects. The results of these tests indicate that force is a function of volumetric constraint. By making the rectangular cut out larger than the enabler, we notice a decrease of output force. For this test, we added a millimeter to the cut out around the enabler. This resulted in an average force of 6.103N, whereas the nominal cut out resulted in an average force of 11.103N. Also, we notice that adding cardboard pieces that take up free space above the enabler in the constraining fixture (between the enabler and the piece of Lexan beneath the force gage), an increase in output force is realized. This force approaches a limit as you reach the minimum free space. That is, as

the free volume goes to zero, the output force approaches its maximum value. We found that placing one piece of cardboard on top of the enabler produced an average force of 6.211N, whereas two layers produced an output force of 11.103. To replicate the realistic function and environment of the enabler, we constrained it using nominal constraints in the x and y-axis, and left a vertical gap of 0.4mm (two layers of cardboard). The force-volume relationship is such that the volume must first be consumed before any force is realized by the force gage. That is, the enabler must consume the free space in the lock before exerting a force.

With the varying parameters, activation time and volumetric constraint, thirty samples were taken on top of the tablet with the full and half sized enabler. The full enabler produced a mean force of 11.103N with a standard deviation of 1.884N, while the half enabler was found to have a mean force of 4.446N with a standard deviation of 1.164N. Normal distributions based upon these estimated parameters are can be found in Figure 29. The solid line represents the full enabler, while the dashed line signifies the half sized enabler.

The data suggests that the full enabler produces more force than the half sized enabler when expanded directly on the surface of the deactivation tablet. This model can be applied to ProTeqt's current USB lock design, which uses the full size enabler on the surface of the tablet. It should be expected that the half sized enabler would produce around half of the force of the full sized enabler. Half of the mean value for the full sized enabler is within one standard deviation of the half sized enabler. The value for the half sized enabler however is not exactly half, as the test apparatus was altered slightly between tests.

The data captured on the surface of the tablet provides a reference to compare the data captured when running the same tests at one inch above the tablet. As with the tests performed on the surface of the tablet, the effect of tablet deactivation time was analyzed with respect to force. (See Figure 30) Unlike the performance on the surface of the tablet, there did not appear to be a peak before one second of deactivation time. We did not observe any burning, and force increased with deactivation time. We believe this to be the result of field decay. This means that as we move further away from the primary coil, it takes longer to heat the enabler.

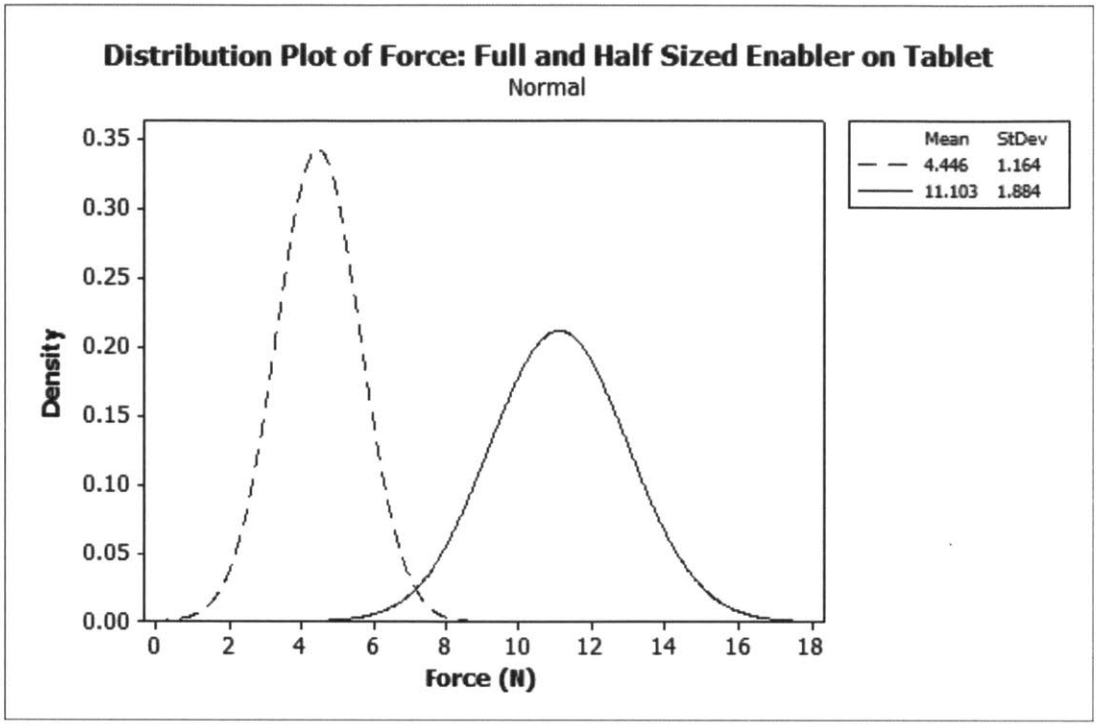

Figure 29: Normal distributions representing enabler force on the tablet.

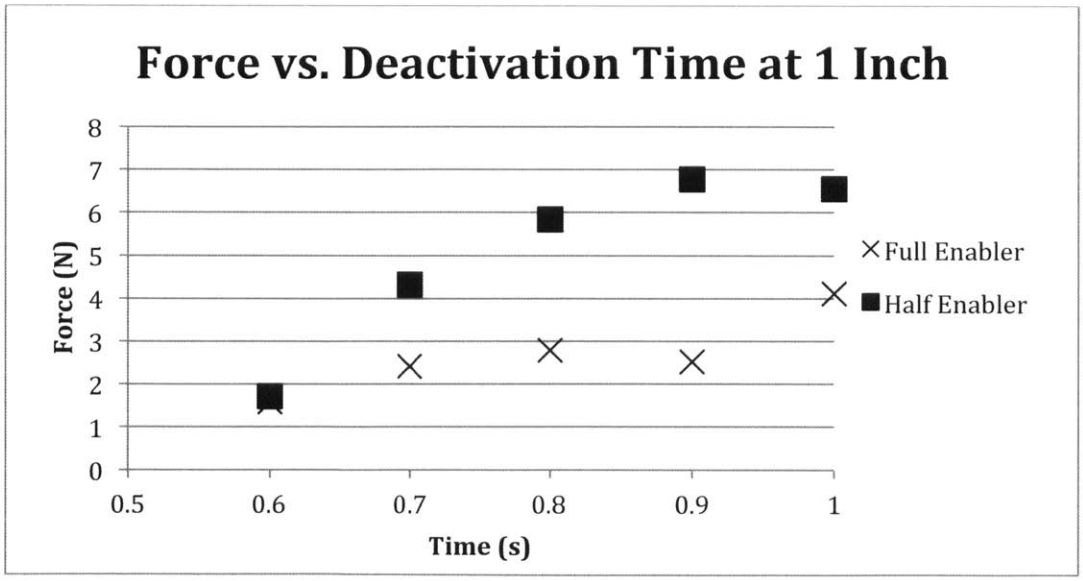

Figure 30: Force vs. deactivation time at one inch.

The tests on the surface of the tablet produced force data from 0.1 to 0.5 seconds, whereas at an inch above the tablet force was produced from 0.6 to 1 second. Forces at time less than 0.6 seconds were insignificant and could not be detected by our

measurement device. Looking at the data, we see that the full enabler fails to produce as much force as its half sized counterpart. The full size enabler does not perform as well as the half sized enabler in this test because it contains a larger thermal mass, and has a larger damping effect on the coupling efficiency of the secondary circuit. The half sized enabler is able to reach a higher temperature than the full sized enabler, and therefore can produce more force.

To maximize the force outputs in future tests, the deactivation time should be maximized (one second). These tests should include gathering larger samples of force at one inch for the full and half sized enabler at one second of deactivation time. Figure 31 shows the normal probability distributions based upon the data samples collected at one inch for the full and half sized enabler, using the solid and dashed lines respectively.

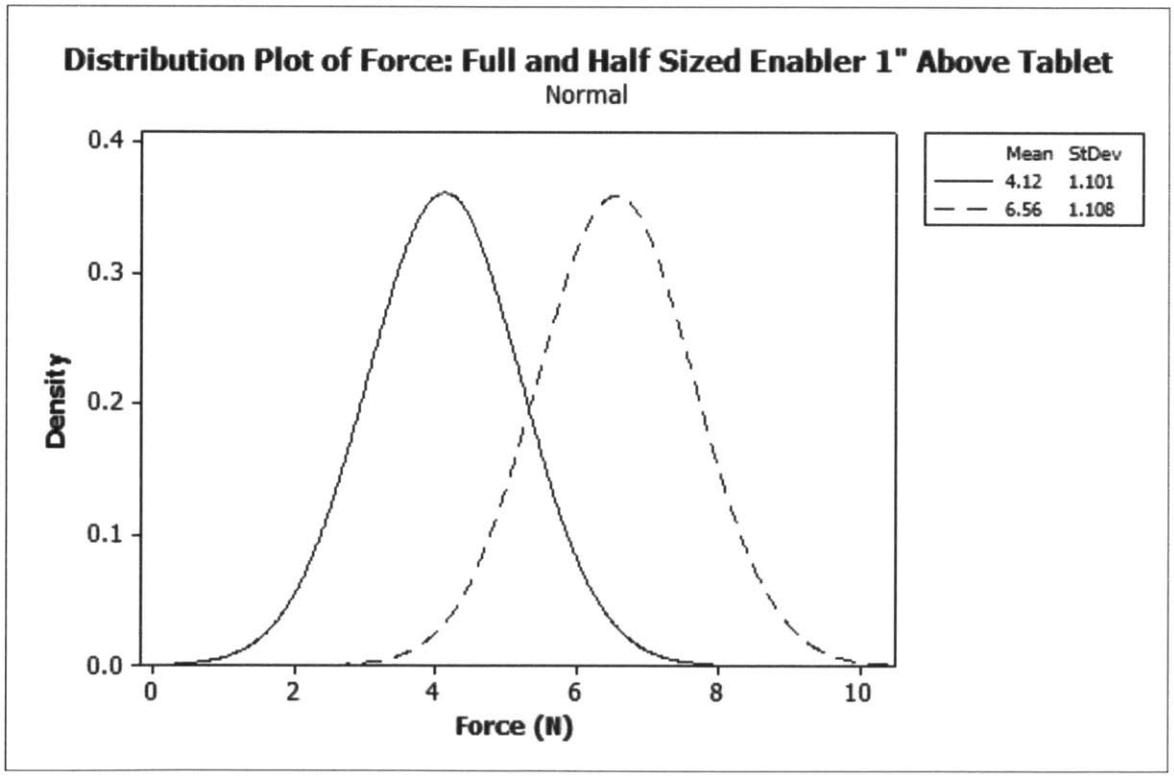

Figure 31: Normal distributions representing full (solid) and half sized (dashed) enabler force at one inch.

Coinciding with our previous tests, the half sized enabler produced more force than the full size. With the half sized enabler, we saw a mean force of 6.56N with a

standard deviation of 1.108N, where as the full size enabler produced a mean force of 4.12N with a standard deviation of 1.101.

Interestingly enough, the half sized enabler actually performs better at one inch than directly on the tablet. The full sized enabler performs better on the tablet than at one inch. This is believed to be a result of distance, heating properties of the system, and the efficiency of the resonant coupling. The field decays exponentially with distance, requiring more time to heat the enabler. That means the rate at which heat is created in the enabler is slower at one inch. With the half sized enabler containing half the thermal mass of the full sized enabler, we can predict that it would perform better in a thermal sense. Finally the efficiency of the resonant coupling is dampened based upon the size of the enabler. The smaller enabler realizes a higher coupling efficiency than its full sized counterpart thus; it is exposed to more eddy currents and is able to heat more effectively.

6.4.4 System Performance

With five distinct data sets, we can begin to compare the force required to disengage the lock with the actual force produced by the full and half sized enablers both on the surface and an inch above the deactivation tablet. As discussed, ProTeqt's benefit denial system should protect consumer products until the point of sale. At the point of sale, the customer should be able to detect a minimal change in the check out process. ProTeqt's system should work seamlessly. The probability that the lock does not disengage should be minimized so that the end customer is never dissatisfied because, after all, ProTeqt's system protects the manufacturer and retailer, not the customer. Customer problems only deter retailers and manufacturers from implementing ProTeqt's system.

Figures 32 through 35 overlay the empirical results of the mean force required to disengage the lock and the force generated under the different conditions of the enabler force tests. Basic intuition says that we should use the enabler that produces the highest force at each condition (on the tablet and an inch above). This will ensure that we have the lowest probability of error, or product failure. In each of the plots, the force required to disengage the lock is depicted by small dashed lines, the force of the half sized enabler is represented by the larger dashed lines, and the full sized enabler uses a solid line.

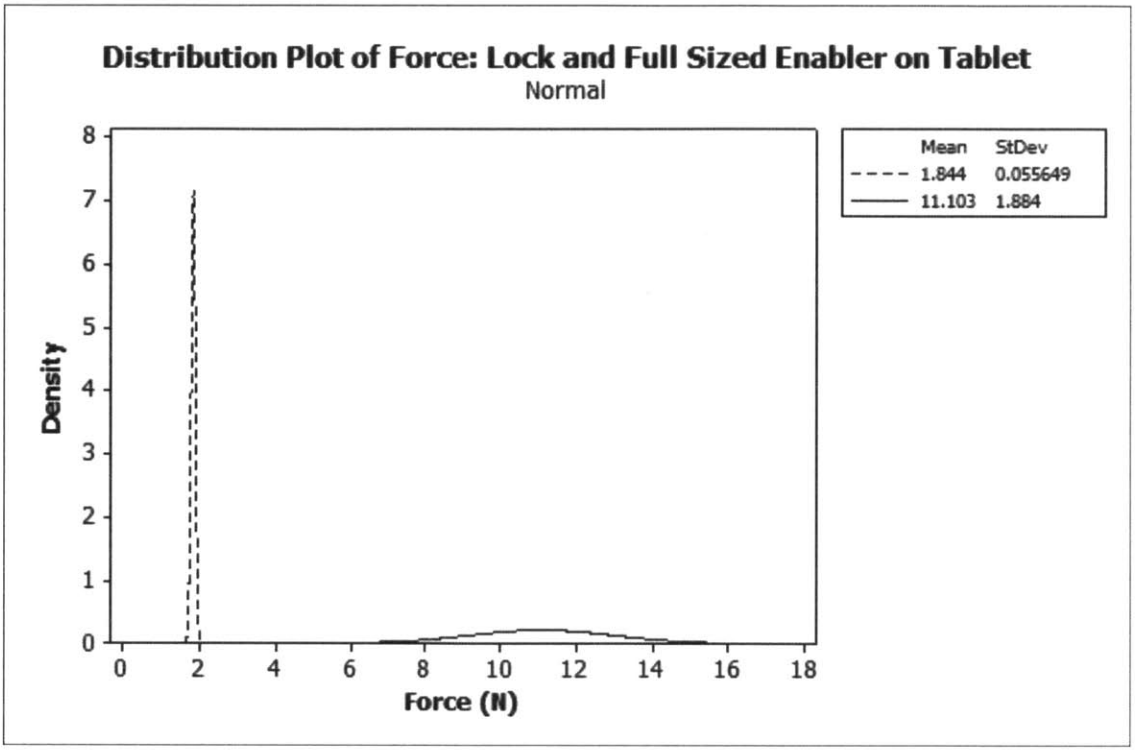

Figure 32: Normal distributions of the disengagement force (dashes) and the force produced by the full sized enabler on the tablet.

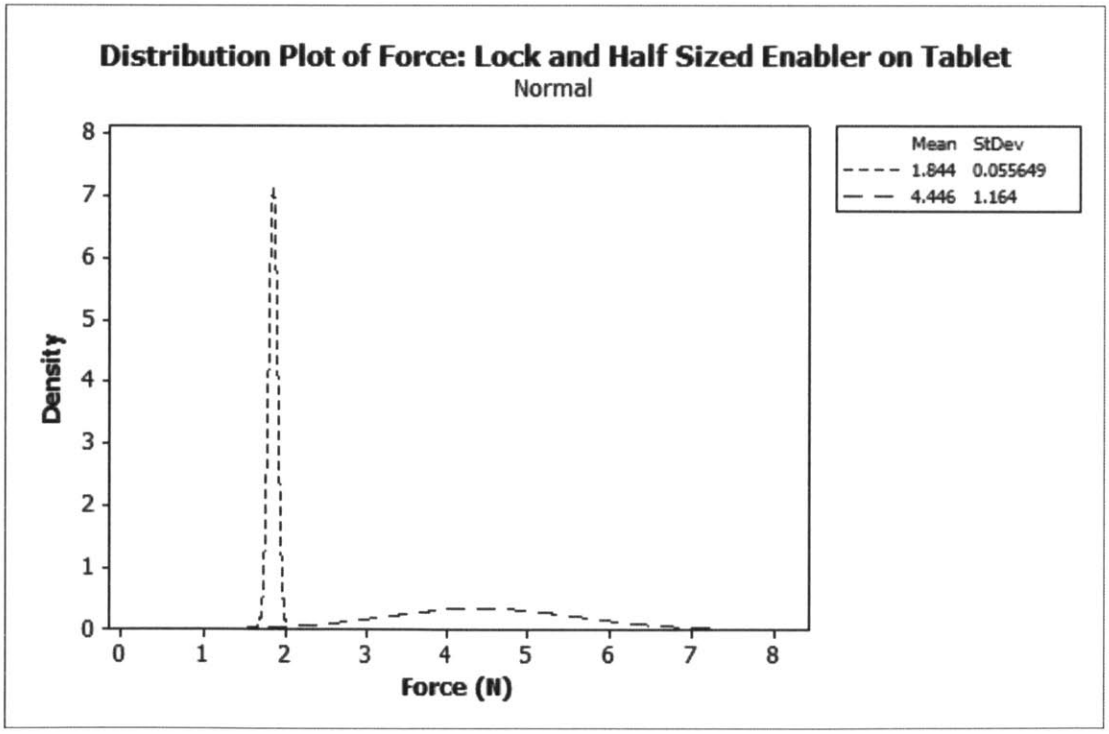

Figure 33: Normal distributions of disengagement force (small dashes) and the force produced by the half sized enabler on the tablet.

Regardless of the logical choice in which enabler to use in each situation, this data provides ProTeqt with a prediction and understanding of the performance of their current mechanical system. The first two plots (Figure 32 and 33) use data taken on the surface of the tablet. While the means of each data set are higher than the force required to disengage the lock, the half sized enabler has a much lower mean. The mean is so low that the standard deviation produces a noticeable overlap between the two distributions in Figure 33. For the robustness of the design, we are concerned with the probability that the system will fail.

By analyzing these plots, we can conclude that the full enabler on the tablet will perform with fewer defects than the half enabler at a distance of one inch above the tablet. This conclusion is based upon the intersecting areas of the distributions. The question becomes, how many defects should ProTeqt expect, and how many defects should they design their system to achieve?

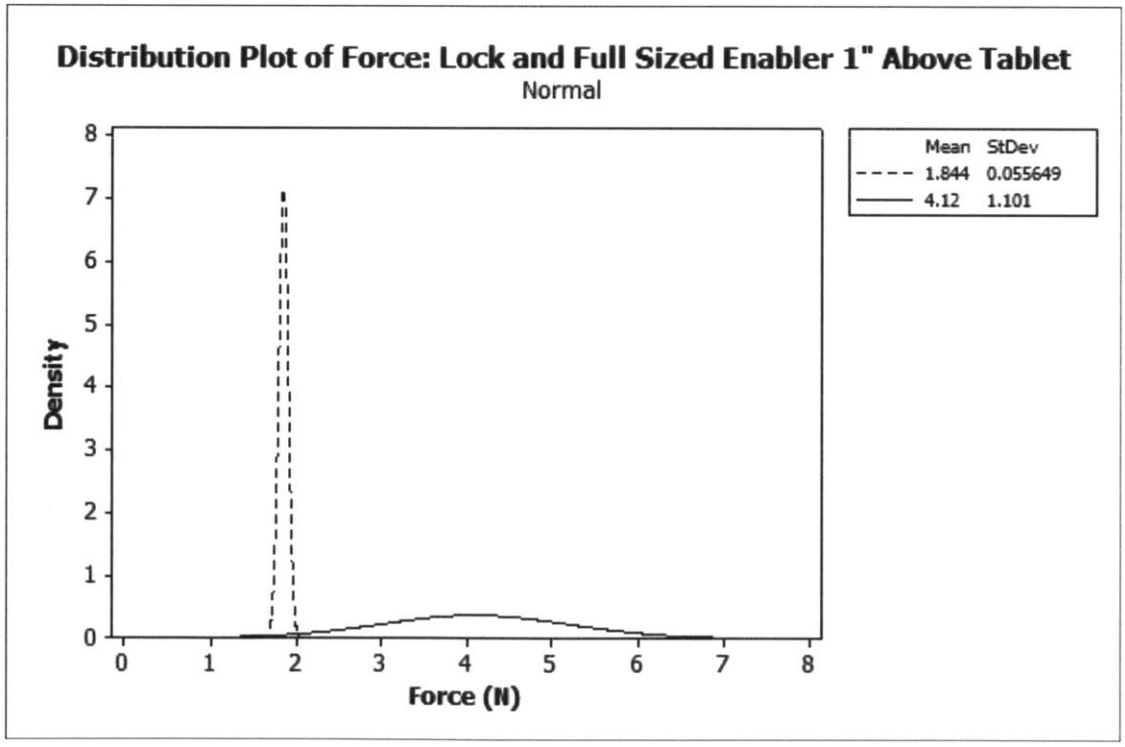

Figure 34: Normal distributions of disengagement force (dashes) and the force produced by the full sized enabler at one inch.

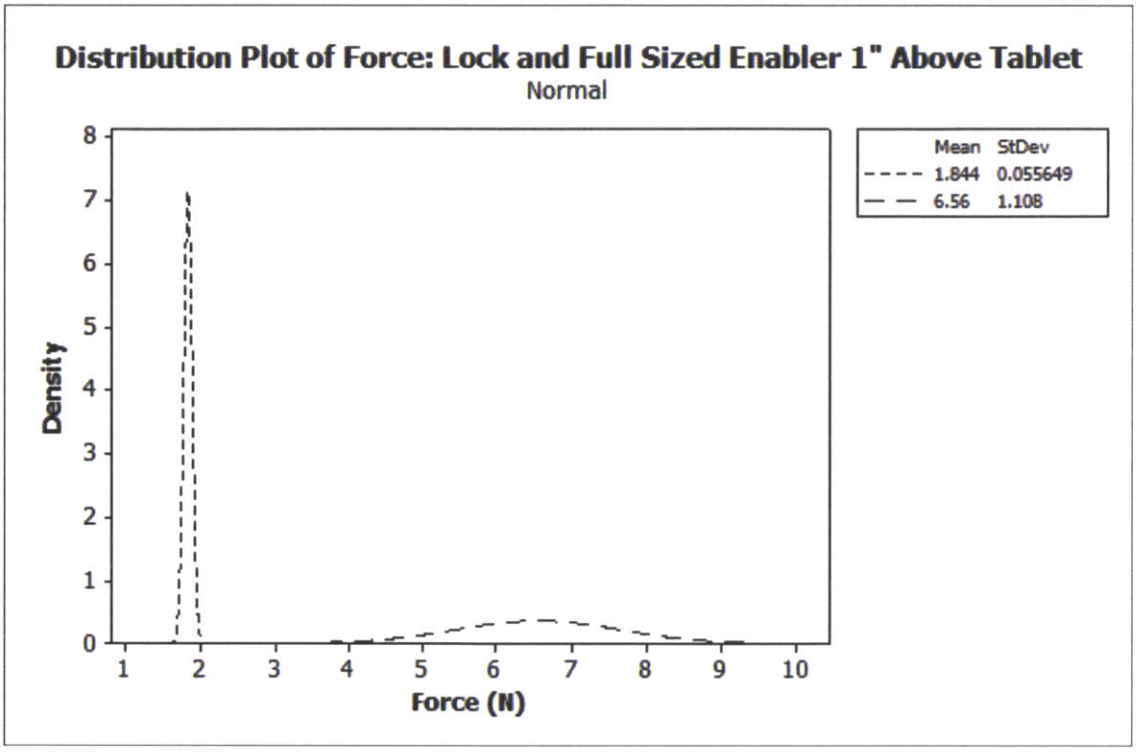

Figure 35: Normal distributions of disengagement force (small dashes) and the force produced by the half sized enabler at one inch.

To estimate the failure rate we consider a new variable: the difference between the disengagement force and the enabler force. By looking at the probability distribution of this quantity , we can calculate the probability that the disengagement force is greater or equal to the force generated by the enabler. Figure 36 further explains the probability function and the failure rate that is calculated. The new random variable is defined as:

$$Y = X_1 - X_2 \tag{6.7}$$

where X_1 and X_2 are respectively the force provided by the enabler and the force required to disengage the locking mechanism.

If X_1 and X_2 are assumed to be normally distributed, Y is also normally distributed with a mean $\mu_Y = \mu_{X_1} - \mu_{X_2}$ and $\sigma_Y^2 = \sigma_{X_1}^2 + \sigma_{X_2}^2$. Since the standard deviation of Y is unknown, the following distribution can be defined:

$$T = \frac{Y - \mu_Y}{s_Y} \sim t(n-1) \tag{6.8}$$

where $n = \min(n_1, n_2)$. n_1 and n_2 are respectively the sample sizes of X_1 and X_2. $t(n-1)$ is the Student's t-distribution with $n-1$ degrees of freedom.

Then, the probability of failure is the probability of Y to be negative:

$$P(Failure) = \mathrm{F}_{t_{n-1}}\left(\frac{0-\mu_Y}{s_Y}\right) \tag{6.9}$$

The numerical values of the failure rate are computed in Table 3.

Table 3: Probability of failure for each of the four deactivation scenarios, with t-distribution.

		μ_Y	s_Y	DoF	Failure Rate
On tablet	**Full**	9.26N	1.88N	29	16.2 ppm[3]
	Half	2.60N	1.16N	29	1.67×10^4 ppm
1 in. above	**Full**	2.28N	1.10N	4	5.39×10^4 ppm
	Half	4.72N	1.11N	4	6.57×10^3 ppm

In this table we see that the probability of failure is reasonably low for a full sized enabler, on the tablet. For the three other situations, the probability of failure is significantly too high for the application of interest. However, in the case of a half sized enabler at one inch above, the failure rate is one order of magnitude smaller than the full sized one. It is believed that this disappointing result come from the insufficiently large sample size for the tests conducted at one inch above. To confirm it, the limit of infinite sample size is computed. In this case, the degree of freedom of the t distribution is $+\infty$, i.e. T follows the standardized normal distribution $\mathcal{N}(0,1)$. The probability of failure becomes:

$$P(Failure) = \Phi_{\mathrm{u}}\left(\frac{0-\mu_Y}{s_Y}\right) \tag{6.10}$$

The results are given in Table 4.

[3] ppm : part per million

Table 4: Probability of failure for each of the four deactivation scenarios, with normal distribution.

		μ_Y	s_Y	Failure Rate
On tablet	**Full**	9.26N	1.88N	0.450 ppm
	Half	2.60N	1.16N	1.28×10^4 ppm
1 in. above	**Full**	2.28N	1.10N	1.95×10^4 ppm
	Half	4.72N	1.11N	10.6 ppm

When comparing the methods, both approaches give similar results when the sample size is 30 (degrees of freedom is 29). However, the results are significantly different for a sample size of 5. Thus, further tests are expected to complete this analysis. A sample size of at least 30 would be preferable.

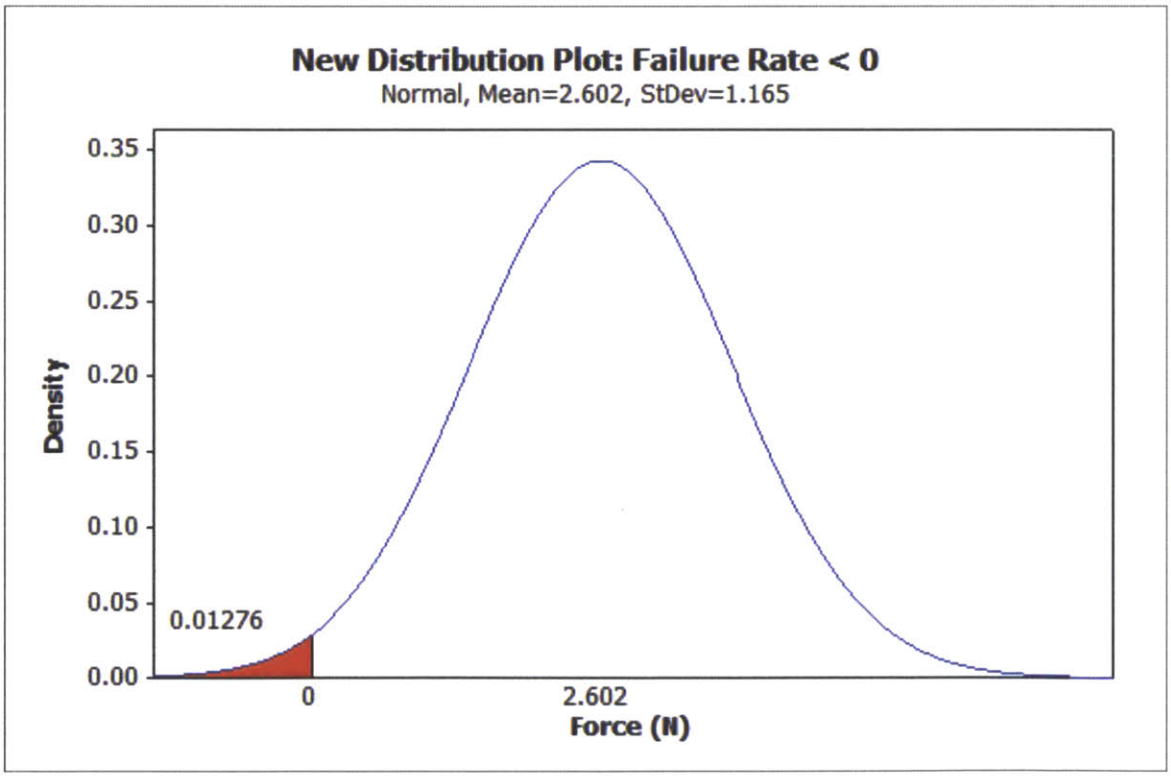

Figure 36: Example of the new calculated distribution and the probability of failure. Visually, the probability of failure is the shaded region of the plot (less than zero).

Chapter 7

LC Circuit Variation and Quality Control

7.1 Objective

The forces generated in the previous section used a fixed LC circuit to create the secondary field that expands the enabler. The actual production on the LC circuit is inherently prone to manufacturing variation nested in the inductor and capacitor. These two components determine the natural frequency of the circuit. In the previous section, we were operating at our target, and best-case scenario, with a natural frequency of 220 kHz. Any shift in natural frequency will result in a less efficient wireless energy transfer, and ultimately less force from the enabler. An analysis of the variation of the inductor and capacitor can be used to measure the total robustness of the system, and establish quality control limits for the components.

7.2 LC Circuit Variation

The optimal LC circuit design from chapter 5 is based on nominal values for inductance and capacitance. As stated before, we must achieve an understanding for the variation in inductance and capacitance to understand the overall performance of the system. These values allow us to complete an analysis of the frequency distribution based on the process variation of the LC circuit.

To determine the variation in the inductance of the coils, we randomly selected ten coils from six different coil batches. These coils were made by a contract manufacturer and mimic actual production practices. We assume that they are a good representation of the variation that ProTeqt can expect when scaling up their production. The inductance of each coil was measured using an LCR meter. The data was first analyzed in groups before being pooled together. By pooling the coils together we achieve an estimate of variance using sixty coils, rather than ten.

As mentioned, capacitors are purchased from a supplier and therefore the variation is estimated using a different method. The capacitors used have a specification of ± 20% of the nominal capacitance rating. In a conservative nature, we assume the

capacitors are normally distributed, and that the specification limits correspond to a six-sigma limit on the capacitance.

Variation of the natural frequency and its impact on the coupling efficiency is controlled by the variation of the inductor and capacitor. A distribution of the natural frequency was calculated based on the distributions of inductance and capacitance. The efficiency was measured in the same method as in chapter 5.

$$Efficiency = I_{load}/I_{source} \tag{7.1}$$

where I_{load} is the current in the LC circuit, and I_{source} is the current through the primary coil. Both of the currents were measured using an oscilloscope.

The maximum efficiency of an LC circuit is independent of its natural frequency. As shown below in the efficiency comparison chart, the two LC circuit with natural frequency 5% below and 15% above 220KHz have almost identical efficiency curves when compared to the 220KHz circuit. Thanks to this characteristic, if the natural frequency of an LC circuit is known, its efficiency on the deactivator is predictable without any testing. If we assume a symmetrical curve, and mirror the efficiency plot of the 220kHz circuit around 220kHz, we can obtain the efficiency plot of coils with various natural frequencies working at 220kHz.

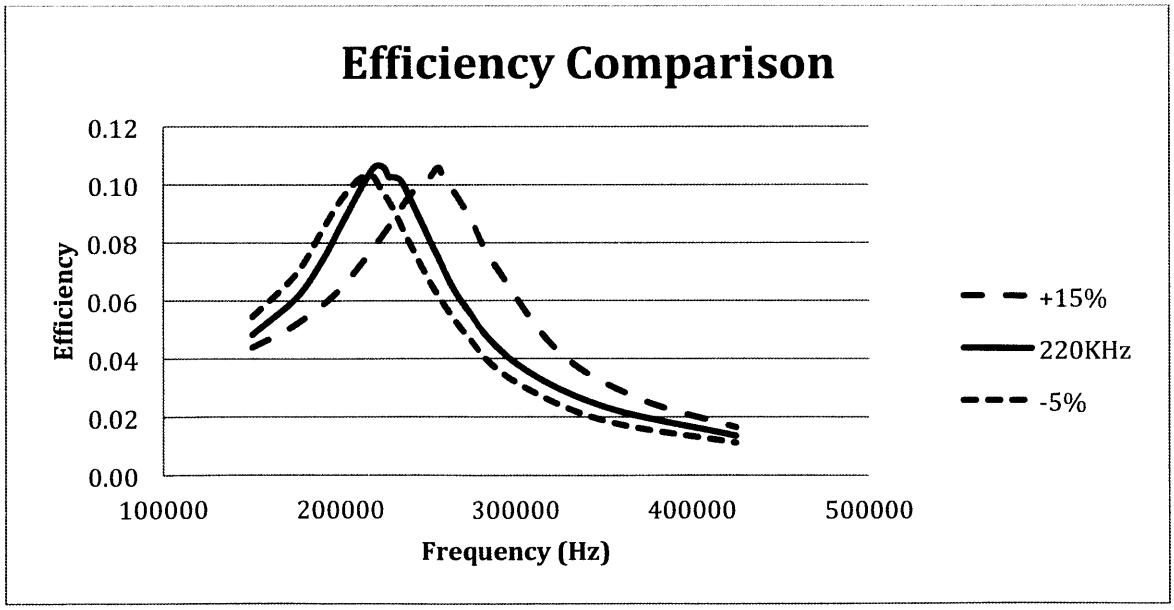

Figure 37: Efficiency plots for circuits with different natural frequencies.

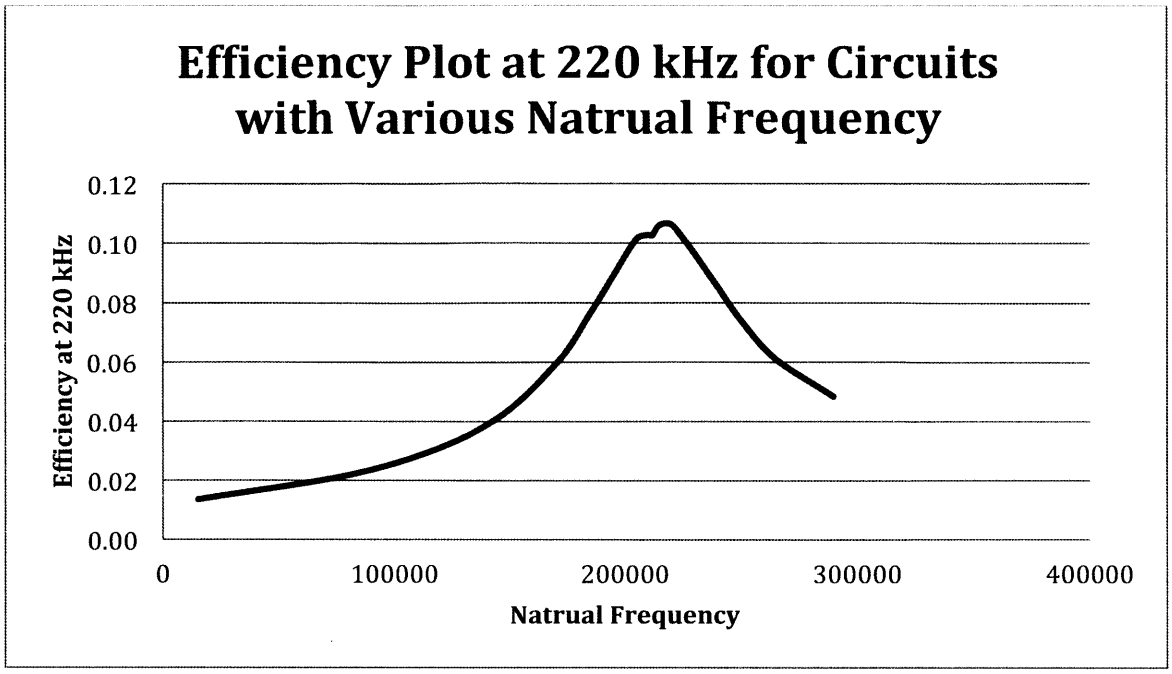

Figure 38: Efficiency plot at 220 kHz for circuits with various natural frequencies.

A linear regression model was then fit based upon the assumption that the curve is symmetrical, with a peak at 220 kHz. More about this process and the regression model please see Tianyu Zhu's thesis [19].

7.2.1 Converting Efficiency to Force

Ultimately the force generated by the enabler is related to the efficiency of the LC circuit. Three circuits were produced at 220 kHz, 15% higher, and 5% lower. Using a production tablet, enabler force tests should be run to understand the differences in output force between the three circuits. The tests should be run in the same fashion as the enabler tests in chapter 6, using each circuit at one inch above the tablet. The unavailability of the production tablet has limited our testing capabilities.

The three data points of the mean force will be enough for ProTeqt to fit a regression model of force with respect to natural frequency. Because the efficiency plot is symmetric about 220kHz, and the force corresponds positively with the efficiency, we expect the force plot to have a similar shape as seen in the efficiency plot.

7.3 Quality Control Limit

By combining the force plots from chapter 6 with the efficiency distribution at 220 kHz for various natural frequencies the total system can be analyzed. With limited access to certain resources like the production tablet, a simulation was conducted to provide initial insight into the total system. The simulation produces a new force curve, taking into account the variability of the LC circuit and the empirical force generated by the enabler. The simulation was computed for the case of the half sized enabler at one inch above the tablet.

7.4 Simulation

A simulation of the enabler performance was conducted to incorporate the effect of varying LC circuits. The simulation is an estimate of total lock performance. Many assumptions were made creating the simulation, and more tests should be carried out to confirm the results.

7.4.1 Simulation Parameters and Setup

Based on the measurement data collected, we assumed that the distribution of inductance L and capacitance C were normal. In the model, the value of inductance and capacitance were generated using the mean (μ_L, μ_C) and standard deviation (σ_L, σ_C) from the samples. The variation of the capacitance is based on the manufacturer specification of 20%. We assume that $\pm 20\%$ is equivalent to six-sigma level.

In the simulation, we assumed a linear relationship between the efficiency (Eff) and mean force (f_{gen}), which can be represented as:

$$\bar{f}_{gen} = \frac{\bar{f}_{gen,max}}{Eff_{max}} Eff \tag{7.2}$$

As observed in the force analysis, the force generated is random due to inherent variation in the enabler. In the model, for every circuit, we use the same CV obtained from force test data (half-size pillow, natural frequency at 220kHz) to calculate the standard deviation (σ_{gen}) of the force. Using the mean force and the standard deviation, a new distribution is created for f_{gen}.

The simulation program requires the following inputs to perform the calculation. The mean and standard deviation of inductance and capacitance measured from actual samples, while the regression model the efficiency plot of the chosen coil is still needed.

Table 5: Simulation input parameters.

μ_L	Mean Inductance	$0.63\mu H$
σ_L	Standard Deviation of Inductance	$0.00665\mu H$
μ_c	Mean Capacitance	$0.1\mu F$
σ_C	Standard Deviation of Capacitance	$0.033\mu F$
f_0	Natural Frequency of LC Circuit	
$\bar{f}_{gen,max}$	Mean Force Generated by the Optimal Circuit	$6.56N$

The program generates a normal distribution of inductance and capacitance using the sample means and standard deviations. The distribution of natural frequency is then calculated by randomly combining inductors with capacitors using their respective distributions. Each of the pairs associates with a respective natural frequency and therefore efficiency. Using the efficiency-force equation (7.2) and σ_{gen}, the force distribution of each coil is obtained. The simulation collects the force distribution associated with each coil, and calculates the collective force distribution. Because force distribution of each coil is assumed to be normal, the overall force distribution is expected to be normal as well. Ultimately, the simulation will used to calculate the probability of failure by comparing the two distributions of force generated and force required. The simulation outputs can be found in table 6.

Table 6: Summary of the simulation outputs.

F_{gen}	Force Generated by the Enabler
$\mu_{F,\ gen}$	Standard Deviation of Force Genrated
P_{fail}	Failure Rate

This simulation was run 3 times, with three different levels of capacitance quality: 5%, 10% and 20%. The objective of the test is to understand how the quality of capacitor

will affect the performance of the system, and, more specifically, the distribution of force generated.

7.4.2 Regression Modeling

15 circuits were assembled to measure natural frequency with the half-size enabler at one-inch distance. The mean natural frequency is 218kHz, proving that the design successfully sets the frequency to the optimal 220kHz. The CV, or ratio of the standard deviation to the mean, of natural frequency calculated at 3.70%, which is higher than that of the inductance and capacitance. This is attributed to stacking up the variation of inductance and capacitance.

With mean square error of only 2.01e-5, the regression model obtained with Minitab is a good representation of the data. The function used for the regression model and a fitted plot can be found in Figure 39. The regression model is the final piece needed for the simulation.

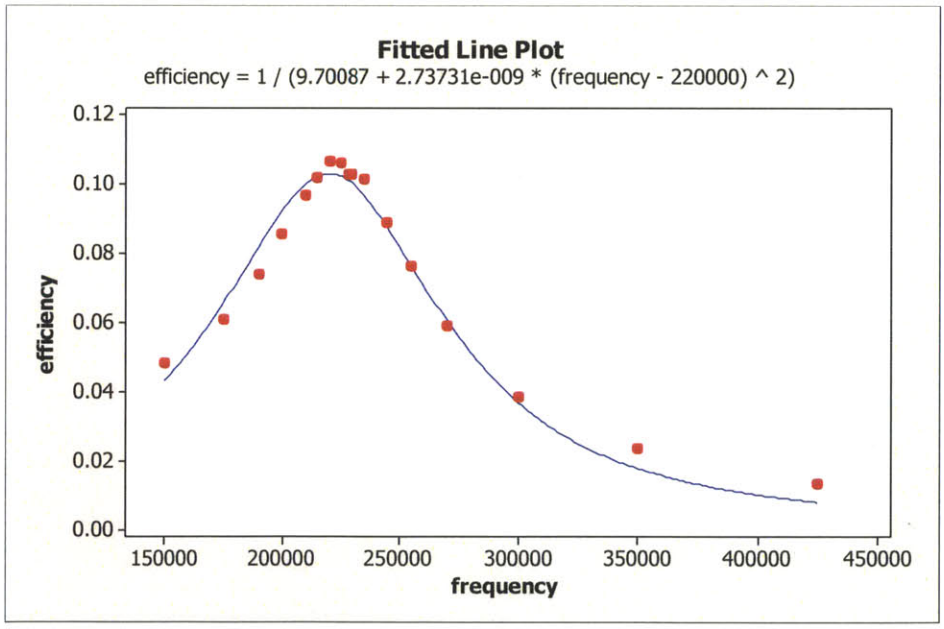

Figure 39: The regression model and fit for circuit efficiency.

7.4.3 Simulation Results

The distribution of natural frequency was simulated using Matlab. As we can see from Figure 40, the natural frequency is normally distributed around 220kHz. The distribution of efficiency, however, is not normally distributed. This is because a circuit

with a higher or lower natural frequency will have a smaller efficiency than the peak at 220 kHz. The histogram of efficiency (20% capacitor) is presented in Figure 41. The distribution has high density around 220kHz, and a long tail toward the left end.

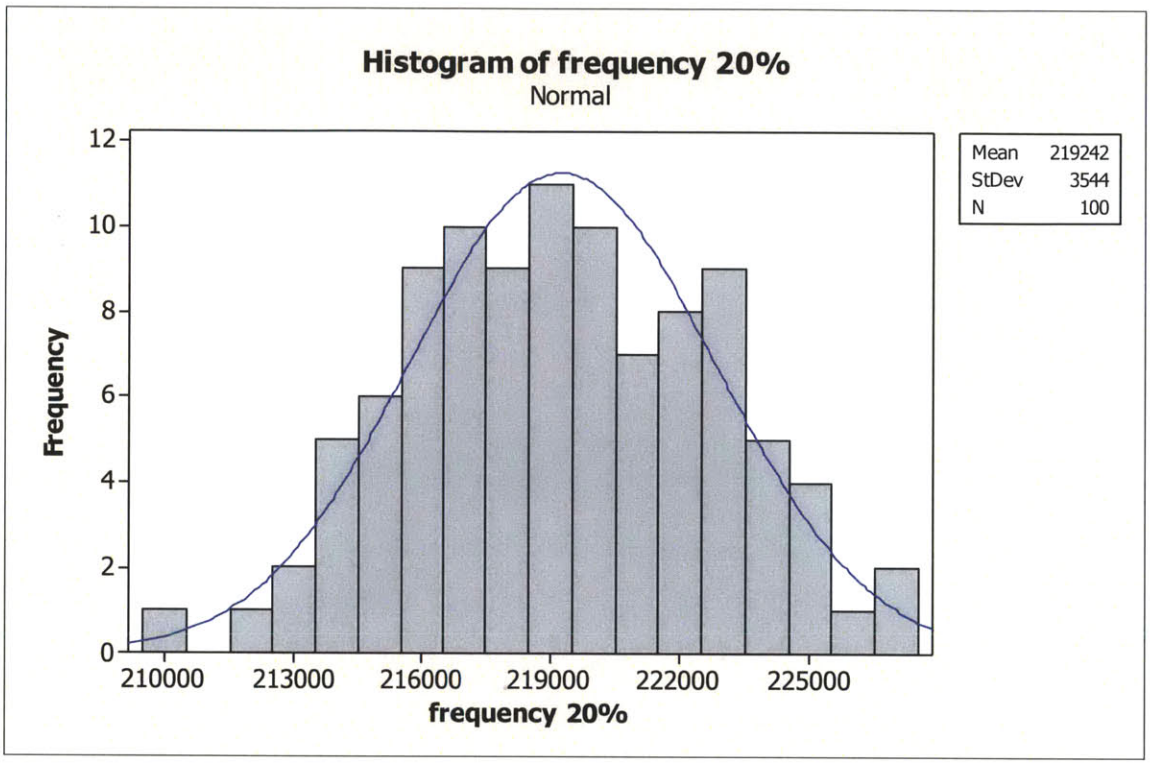

Figure 40: Histogram of natural frequency (20% Capacitor).

The histogram of the force distribution (20% capacitor) exhibited in Figure 42 is normally distributed as expected.

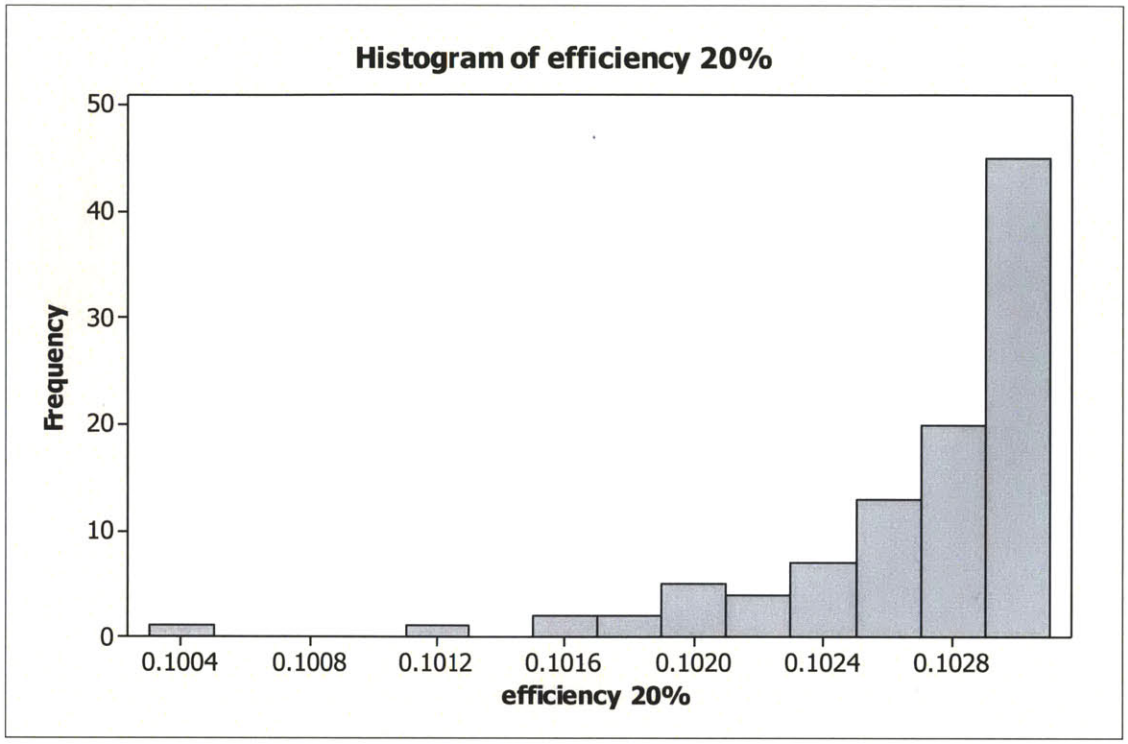

Figure 41: Histogram of efficiency (20% Capacitor).

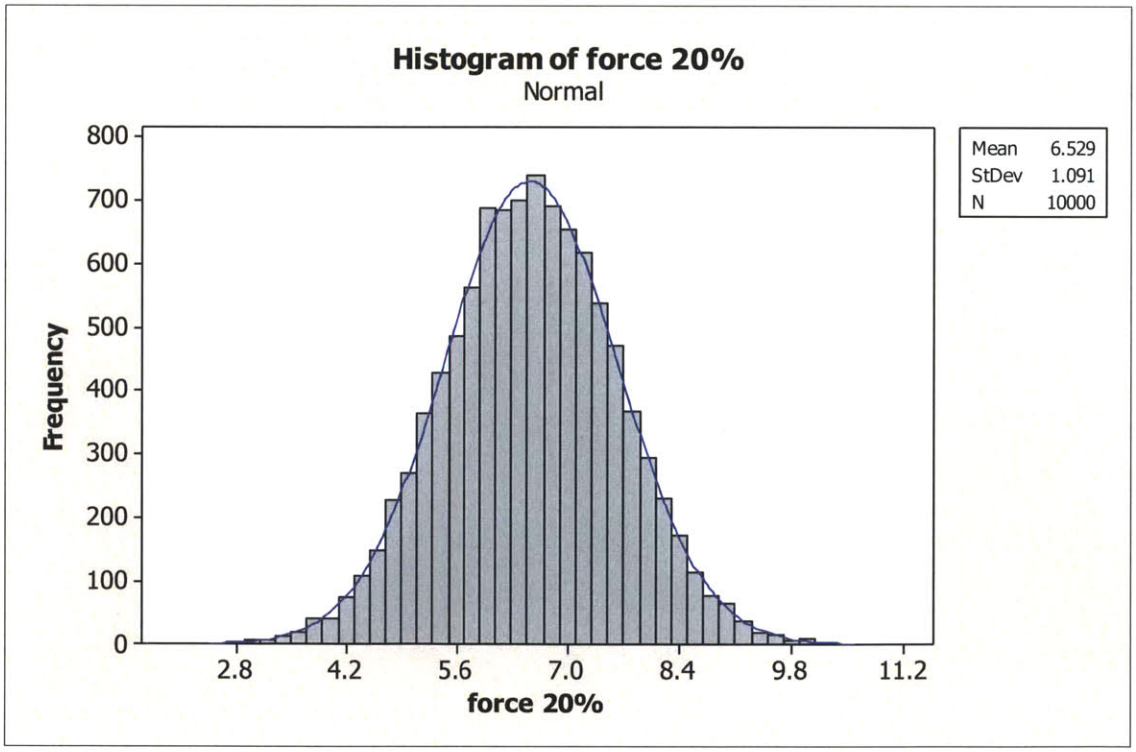

Figure 42: Histogram of the force generated by the half sized enabler.

According to the simulation result, we found that the force generated by the enabler is significantly higher than the 1.844N force needed to disengage the lock even with the 20% capacitor. The results of the sensitivity analysis of the capacitors are shown in Tables 7 and 8.

Table 7: Resonant frequency distributions based on capacitor quality.

Cap. Quality	5%	10%	20%
Mean	219,469 Hz	219,585 Hz	219,242 Hz
Standard Deviation	1,018 Hz	2,095 Hz	3,544 Hz
95% CI for mean	[219,266 ; 219,271]	[219,169 ; 220,000]	[218,782 ; 221,069]
95% CI for std. dev.	[894 ; 1,183]	[1,840 ; 2,434]	[3,112 ; 4,117]

Table 8: Force distributions based on capacitor quality.

Cap. Quality	5%	10%	20%
Mean	6.5527 N	6.5497 N	6.5295 N
Standard Deviation	1.1005 N	1.1015 N	1.0909 N
95% CI for mean	[6.5311 ; 6.5743]	[6.5281 ; 6.5713]	[6.5081 ; 6.5509]
95% CI for std. dev.	[1.0854 ; 1.1159]	[1.0864 ; 1.1170]	[1.0760 ; 1.1062]

As expected, the standard deviation of the frequency distribution increases as the capacitor quality decreases. However, under our assumptions, it does not affect the standard deviation of the enabler force distribution. The 95% confidence intervals for the standard deviations overlap. In the particular case of this realization, the estimate of the standard deviation for 20% capacitor is even smaller than the 5 and 10% capacitors. This phenomenon is attributed to the rather large manufacturing variability of the enablers. Thus, the force distribution that is generated has a significantly higher variance than the electronic components. From this simulation we find that the using the 20% capacitor would be an acceptable component for the circuit. This simulation reinforces the importance of reducing manufacturing variability of the enabler. Manufacturing of the enablers are currently made by hand and manufacturing control of this part is not a priority for ProTeqt yet. As a final result of the simulation, we combine the ideology of the previous chapter and compute a failure rate based upon the mean and standard

deviation of the total system using the 20% capacitor. Reiterating the fact that this is indeed a simulation with many assumptions, we generate a new distribution using the force required to disengage the lock. Assuming that everything is normally distributed, we find the failure rate to be about 9 parts per million using the half sized enabler at 1 inch. For more information on the simulation and the variance of the total lock system, please refer to Tianyu Zhu's thesis [19].

Chapter 8

Conclusions

After working with ProTeqt Technologies on their benefit denial solution for the retail industry, the most important conclusion we can draw is that their solution can successfully be applied to products requiring embedded packaging that extend the lock to a distance of one inch above the deactivation tablet by using a resonantly coupled LC circuit. Within the realm of deactivation at distance, we have drawn many other conclusions throughout the project.

Focusing on the LC circuit, we conclude that there are several factors that should be considered when designing the circuit; some of the most important for this application include shape, size, and natural frequency. Many of these parameters are limited depending on the manufacturing processes used to make the circuit. We conclude that a coil winding process should be used to manufacture the inductor component of the LC circuit because it is a tried and true process that can produce coils at a very low cost. With an LC circuit containing a wound coil inductor, optimization declared that the best circuit, given the constraints already inherent in ProTeqt's lock design, would use a copper coil that has a 24 Gage wire diameter and 9 turns. The inductance of this coil combined with a 1 micro-farad capacitor would achieve the proper natural frequency that would provide a sufficient resonant coupling to create a strong enough magnetic field to deactivate the lock at one inch.

Using the optimized LC circuit design, we found that the lock could be optimized to better facilitate deactivation at one inch. By examining the forces produced by the enabler, we found that when working directly on the tablet, the full sized enabler produces a larger force than the half sized enabler. However, at a distance of one inch we found that the half sized enabler could produce a larger force. This phenomenon occurs because when unlocking devices on the tablet, ProTeqt is simply over powering the system. At one inch, thermal properties and coupling efficiency become very important. The half sized enabler has half of the thermal mass as full sized enabler. Therefore, the half sized enabler can reach the required temperature must faster than the full sized enabler. Also, the half sized enabler has less of a damping effect on the coupling

efficiency between the primary coil and LC circuit, producing a stronger magnetic field, and therefore the ability to generate more heat.

After analyzing the force generated by the full and half sized enabler on the tablet and at a distance of one inch we decided to understand the forces required to disengage the lock. Empirically and analytically we conclude that the force required to disengage the lock is less than 4N. This was the theoretical maximum found using an FEA and an analytical calculation. Empirically we found the force required to disengage the lock to be around 1.8N.

By combining data sets the probability of failure due to the enabler was analyzed to better understand the sources of failure in the total system. On the surface of the tablet, using the full sized enabler, we found the expected failure rate to be 0.45 parts per million. At one inch the half sized enabler produced a failure rate of 10.6 parts per million, with a limited data set. These probabilities are reasonably low, however in reality we notice the product failing far more often because of other issues such as the performance of the deactivation tablet and the sensitivity to the relative position between the primary and secondary coil.

To gain a better understanding of the entire lock performance, including the variability of the LC circuit at one inch, we developed a simulation model to predict the shift in performance based on the natural frequency of the circuit. In the end, we concluded that the capacitor was likely the component of the LC circuit that would add the most variability with respect to natural frequency. The simulation model related a peak shift in natural frequency to a resulting force exerted by the enabler. While we did obtain an output, it's the process that ProTeqt should be interested in. The simulation was based on many assumptions, and found that even with a large peak shift, the efficiency of the energy transmission was enough for the circuit to produce failure rates on the order of 10 parts per million.

Chapter 9

Future Work

Drawing from the conclusions of this thesis, ProTeqt's future work can be divided into short and long-term work. Short-term work is more applicable to the thesis at hand and long-term work is much more future facing.

9.1 Short-term

First and foremost, the design and development of the deactivation tablet should be completed. The deactivation tablet is the most unpredictable and unreliable component in ProTeqt's entire system. To satisfy customers it should be as reliable as the lock. A failed deactivation due to any component, whether it be the lock, database, or deactivation tablet, will be dis-satisfying to customers and drive away their solution. Added benefits of a fully functioning, reliable deactivation tablet include a better understanding of the tablet and it's inputs and outputs, reliable test results, and customer trials and simulations.

With or without a working tablet, ProTeqt should work to understand and lockdown a "thin wire" design. The copper spiral inductors used for this project are large and tangible. A "thin wire" design would imply the feasibility and opportunity to use other manufacturing methods like etching or printing. This is future facing design task, because over time the cost of these manufacturing processes will become more competitive with coil winding.

Using ProTeqt's existing tablet setup, they can design experiments and test to see if different types of enablers would work better, or if the enabler could be optimized for different applications. We analyzed the half sized enabler and compared the results with the full size. Other opportunities include analyzing larger and smaller sized enablers, different shapes and sizes, and ultimately different materials. We hypothesize that the corners of the enabler act as extra thermal mass, and that the eddy currents would be more efficient in a circular conductor. This could make the wireless energy transfer even more efficient with less thermal mass and possibly less of a damping effect on the LC circuit.

9.2 Long-term

In the long term ProTeqt should be examining different opportunities that would allow them to further extend the working distance of the lock. Working at an inch is great, however larger embedded packaging challenges exist. Many of these larger products are also of high value, like televisions for example. High value products could give ProTeqt an opportunity to create locks at a higher cost. More sophisticated solutions should be developed to accommodate some of the future opportunities.

Ultimately, ProTeqt should think about how they can position themselves to be involved with a software lock. That is, a product could be purchased with out a mechanical lock. Instead the product is not functional because the internal software will not work until it passes through the point of sale. To accommodate this idea, the deactivation tablet is key. By getting their product to market and in stores, they could have the infrastructure in place to help this feature progress in the electronics retail industry.

Bibliography

[1] K. Finklea, *Organized Retail Crime*. Congressional Research Service, 2011.

[2] Centre for Retail Research, "Centre for Retail Research, Nottingham UK," *The First Worldwide Shrinkage Survey*, 2011. .

[3] R. M. Sutton, *Demonstration Experiments in Physics*. McGraw-Hill company inc.

[4] M. Zahn, *RES.6-002 Electromagnetic Field Theory: A Problem Solving Approach, Spring 2008. (Massachusetts Institute of Technology: MIT OpenCourseWare), License: Creative Commons BY-NC-SA*. 1987.

[5] K. Finkenzeller, *RFID Handbook: Fundamentals and Applications in Contactless Smart Cards and Identification*. John Wiley & Sons, Inc., 2003, p. 446.

[6] M. J. Schauber, S. A. Newman, L. R. Goodman, I. S. Suzuki, and M. Suzuki, "Measurement of mutual inductance from frequency dependence of impedance of AC coupled circuits using a digital dual-phase lock-in amplifier E ~ Lock-in ampliier," *American Journal of Physics*, vol. 76, no. 2, 2007.

[7] N. Tesla, "Apparatus for Transmission of Electrical Energy," 1900.

[8] A. Kurs, A. Karalis, R. Moffatt, J. D. Joannopoulos, P. Fisher, and M. Soljacic, "Wireless power transfer via strongly coupled magnetic resonances.," *Science (New York, N.Y.)*, vol. 317, no. 5834, pp. 83–6, Jul. 2007.

[9] A. Karalis, A. B. Kurs, R. Moffatt, J. D. Joannopoulos, P. H. Fisher, and M. Soljacic, "Wireless energy transfer," 2009.

[10] S. V. Georgakopoulos and O. Jonah, "Optimized wireless power transfer to RFID sensors via magnetic resonance," *2011 IEEE International Symposium on Antennas and Propagation (APSURSI)*, pp. 1421–1424, Jul. 2011.

[11] B. Cannon and J. Hoburg, "Magnetic resonant coupling as a potential means for wireless power transfer to multiple small receivers," *IEEE Transactions on Power Electronics*, vol. 24, no. 7, pp. 1819–1825, 2009.

[12] L. Beckwith, "Inductor Theory," *General Linear Systems*, 2013. .

[13] Y. Lee, "RFID Coil Design," 1998.

[14] P. Universe, "Printed circuit boards," *PCB Universe*, 2013. [Online]. Available: http://www.google.com/patents?hl=en&lr=&vid=USPAT4751146&id=9lIyAAAA

EBAJ&oi=fnd&dq=Printed+Circuit+Boards&printsec=abstract. [Accessed: 27-Jul-2013].

[15] A. SAWYER, "Fabrication of nanofluidic devices using electrochemical etching of sacrificial copper," 2010.

[16] "Red C12000 Oxygen Free Copper Wire," 2013. [Online]. Available: http://www.alibaba.com/product-gs/430200636/Red_C12000_Oxygen_Free_Copper_Wire.html.

[17] M. Hoban and B. Lunt, "Soldering," *The Technology Interface*, May-1997. [Online]. Available: http://www.ncbi.nlm.nih.gov/pubmed/23822908.

[18] D. Numakura, "Advanced Screen Printing 'Practical Approaches for Printable and Flexible Electronics'," *2008 3rd International Microsystems Packaging Assembly Circuits Technology Conference*. Ieee, pp. 205–208, 2008.

[19] T. Zhu, "Design and Manufacturing Analysis of Resonantly Coupled Circuits and Other Components used for Wireless Benefit-Denial System," Massachusetts Institute of Technology, 2013.

[20] A. Rony, "Analysis and Design of Resonant Inductively Coupled Circuits: Application to Benefit Denial Solutions for the Retail Industry," Massachusetts Institute of Technology, 2013.

[21] "Friction and Coefficients of Friction," 2013. [Online]. Available: http://www.engineeringtoolbox.com/friction-coefficients-d_778.html.

Appendix A: FEA Results at Different Loads

The figures included in Appendix A are the finite element analysis results that are not included in the main text of the thesis. The analysis was used to estimate the bending force required to disengage the lock. Originally we were concerned with achieving a displacement of about 0.4mm. Ultimately, we believe a displacement of 0.1mm is actually necessary to disengage the lock. To run the analysis, we completed many FEA load scenarios included in this appendix.

We found that a 4N load was required to achieve 0.1mm of displacement in the component. More information on the FEA, including loads and constraints can be found in Chapter 6: specifically Figures 20, 24, and 27. The figures below include a color-coded chart that corresponds to the displacement found in the part. The measurements are in millimeters.

FEA result with 5N load.

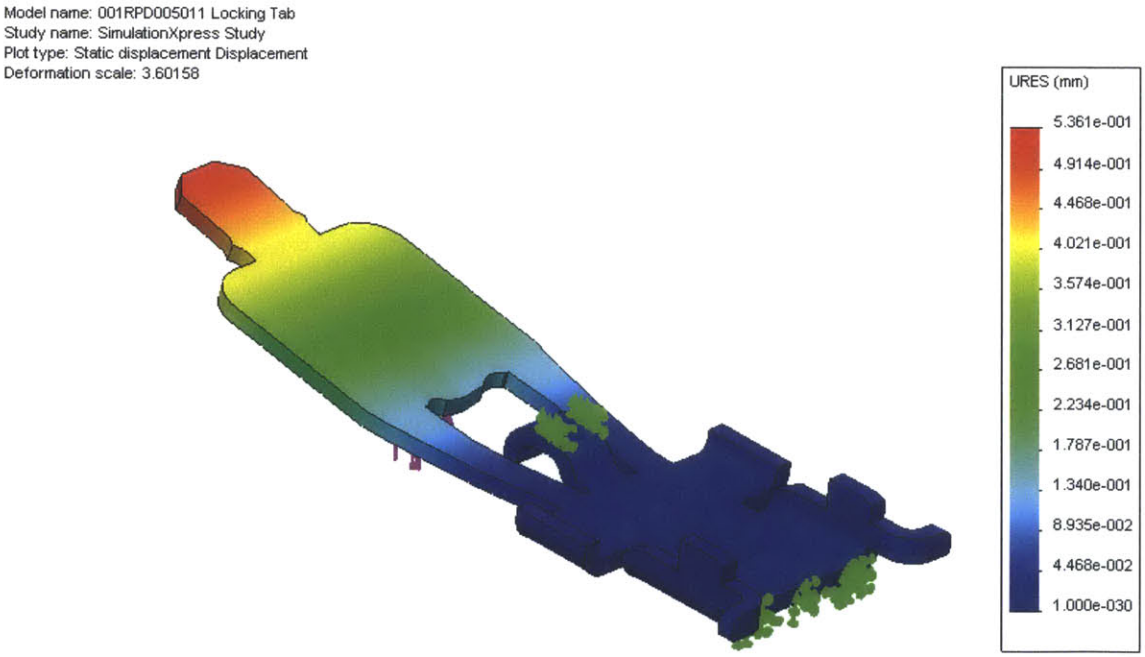

FEA result with 10N load.

Model name: 001RPD005011 Locking Tab
Study name: SimulationXpress Study
Plot type: Static displacement Displacement
Deformation scale: 1.80079

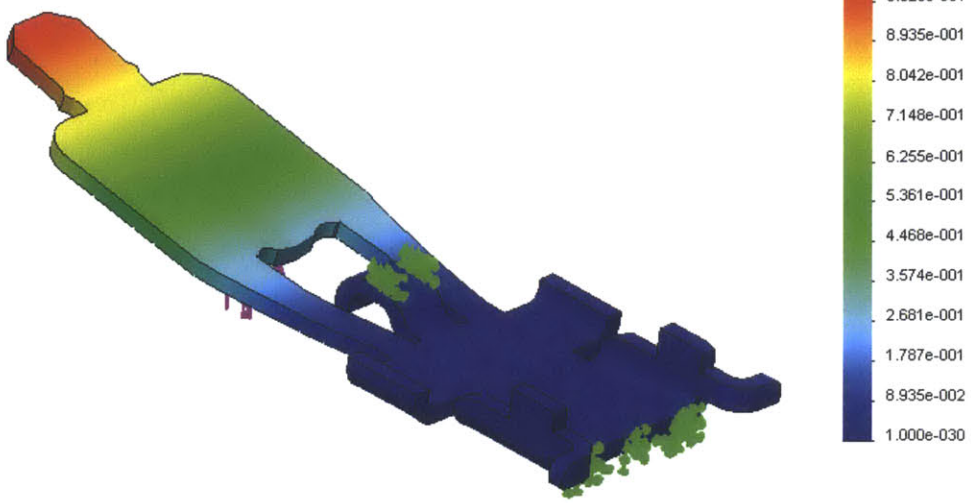

FEA result with 20N load.

Model name: 001RPD005011 Locking Tab
Study name: SimulationXpress Study
Plot type: Static displacement Displacement
Deformation scale: 0.900394

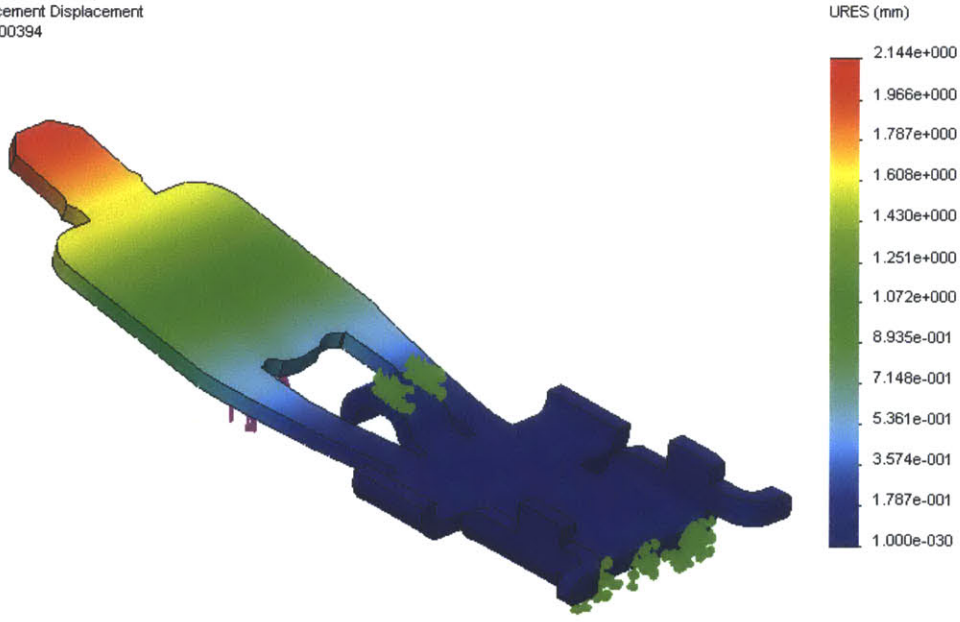

Appendix B: Probability Plots of Empirical Data

The normal probability plots included in this appendix reinforce our assumption that the measured data that collected throughout the project is normally distributed. The first plot describes the force required to disengage the locking mechanism. We took 30 data points for this test. We see that the data is centered on a mean of 1.844N.

The four remaining plots are of the forces produced by the enabler. The four scenarios are full and half enabler, on and an inch above the tablet. On the tablet we were able to observe 30 and 18 tests respectively for the full and have enabler. The tests an inch above the tablet included 5 data points for the full and half sized enabler. Only taking 5 data points is not ideal. More tests should be run to reinforce the normal assumptions for the tests at an inch above the tablet.

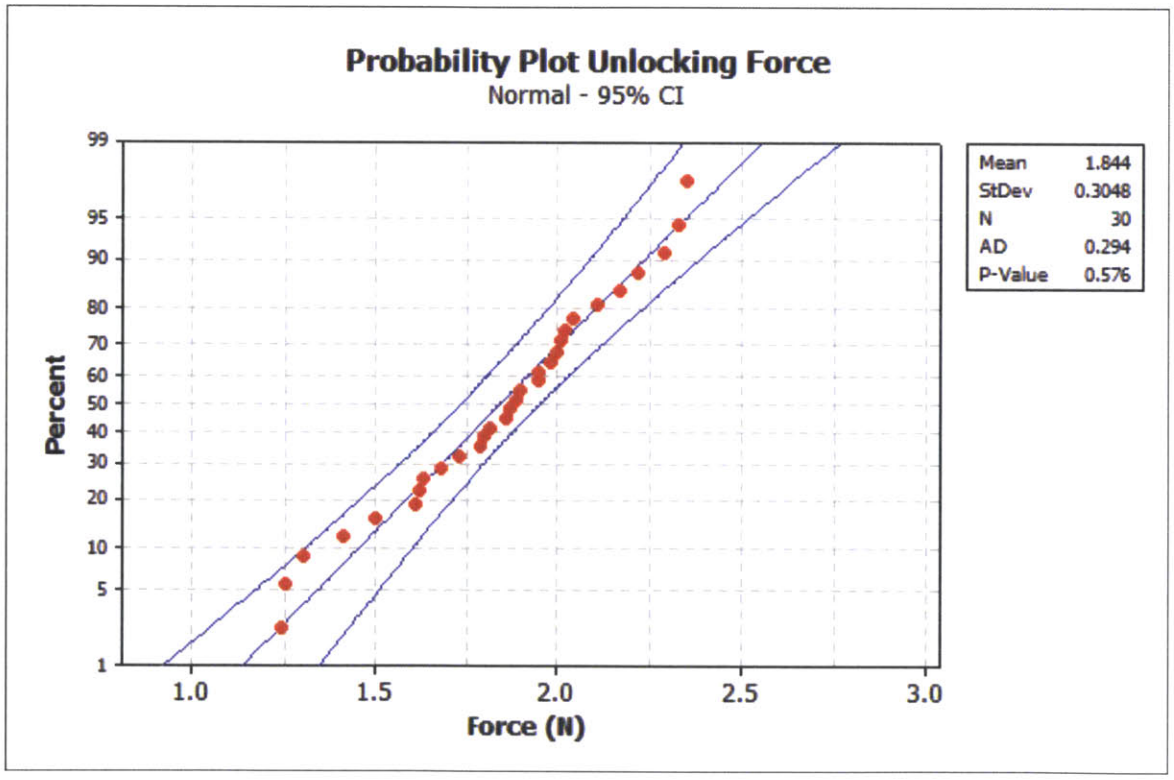

Probability plot for the unlocking force. P-value is greater than 0.05, therefore we assume the data to be normally distributed.

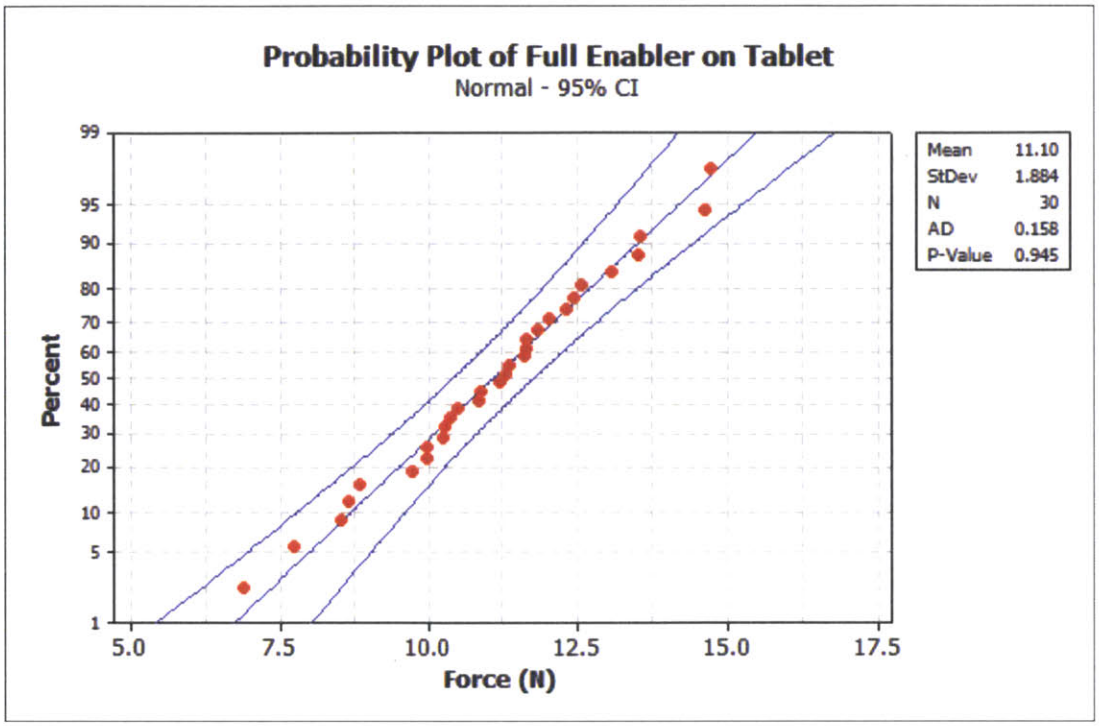

Probability plot for the force generated by the full enabler on the tablet. P-value is greater than 0.05, therefore we assume the data to be normally distributed.

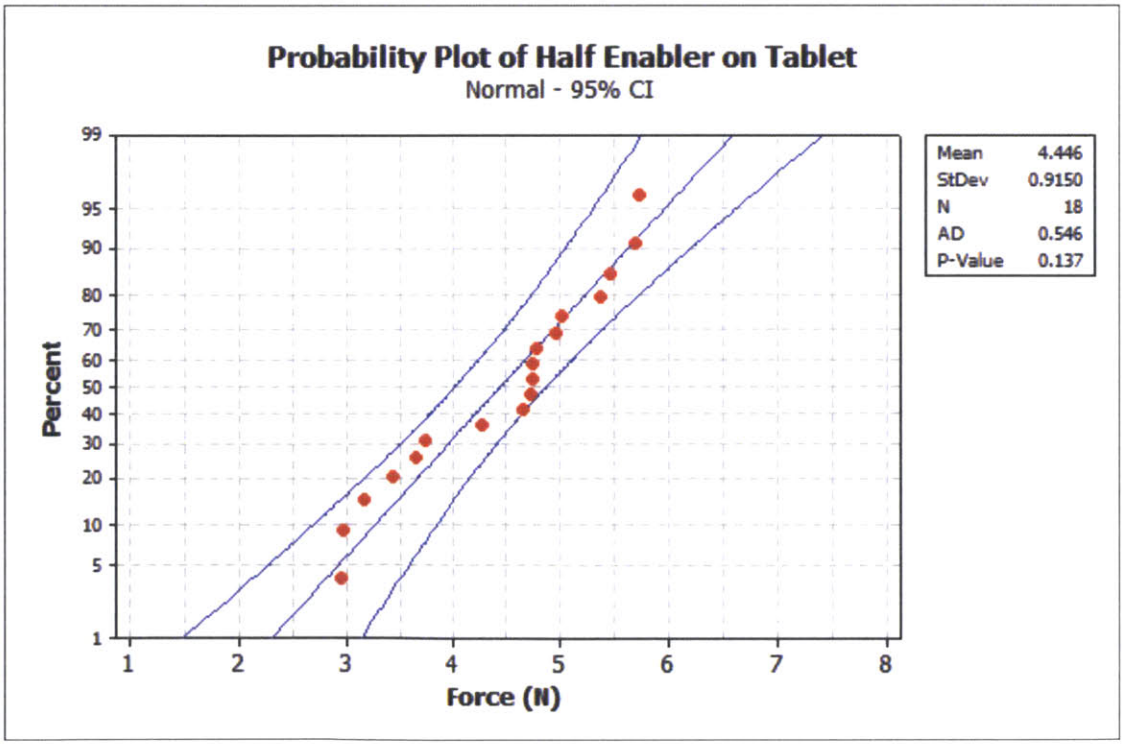

Probability plot for the force generated by the half enabler on the tablet. P-value is greater than 0.05, therefore we assume the data to be normally distributed.

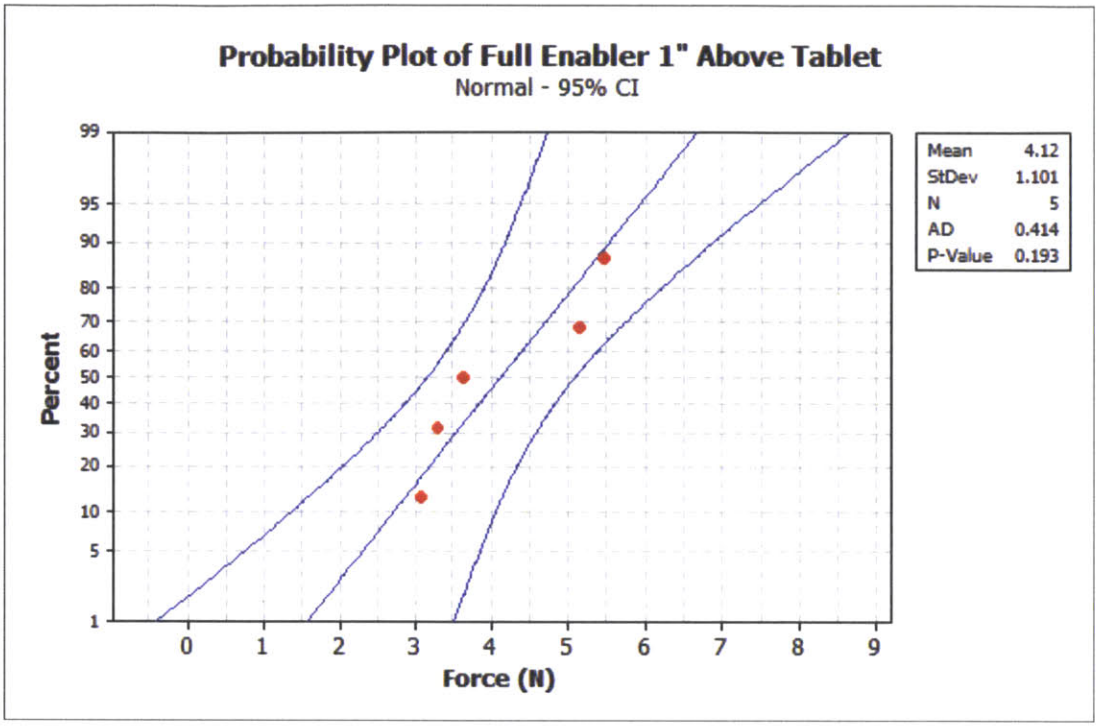

Probability plot for the force generated by the full enabler 1" above the tablet. P-value is greater than 0.05, therefore we assume the data to be normally distributed.

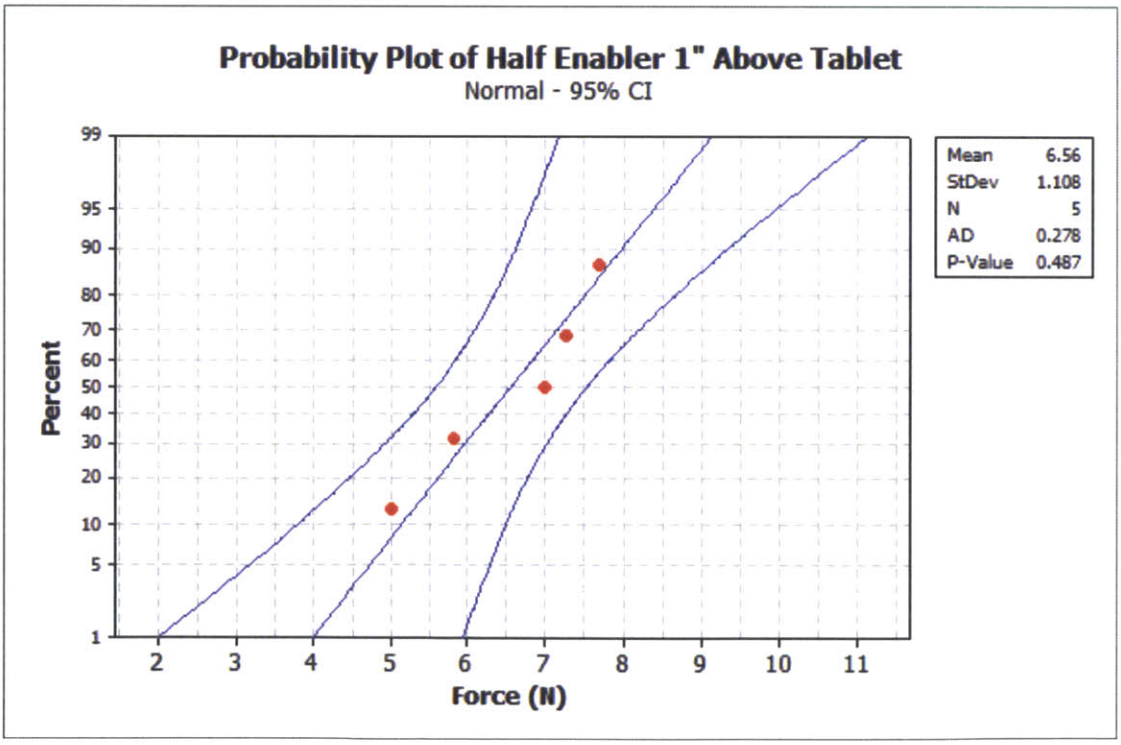

Probability plot for the force generated by the half enabler 1" above the tablet. P-value is greater than 0.05, therefore we assume the data to be normally distributed.